Agricultural Water Management 305 (2024) 109127

Contents lists available at ScienceDirect

Agricultural Water Management

journal homepage: www.elsevier.com/locate/agwat

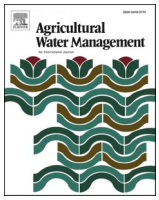

# Measurement and modelling of Moringa transpiration for improved irrigation management

Ambroise Ndayakunze [a,b], Joachim Martin Steyn [b,*], Christian Phillipus du Plooy [a], Nadia Alcina Araya [a,1]

[a] Agricultural Research Council, Vegetable, Industrial and Medicinal Plants, Pretoria, South Africa
[b] University of Pretoria, Department of Plant and Soil Sciences, Pretoria, South Africa

ARTICLE INFO

Handling Editor - Dr Z Xiying

*Keywords:*
Canopy conductance
EXO-Skin sensors
Plant-based water monitoring
Sap flow
Stem heat balance

ABSTRACT

A greater understanding of Moringa (*Moringa oleifera* Lam.) transpiration (T) can assist in the development of accurate irrigation management tools. This study aimed at quantifying Moringa T by measuring and modelling the sap flow (SF) of intact stems using an improved heat balance technique. The study was conducted during two consecutive seasons (2021–2022 (Season 1) and 2022–2023 (Season 2)) at the Roodeplaat Experimental Farm of the Agricultural Research Council in South Africa. EXO-Skin sap flow sensors were used. Transpiration-related drivers such as weather and plant physiological parameters were measured simultaneously. The measured SF data in Seasons 1 and 2 were used to respectively parameterize and validate a canopy conductance T model. There was a positive correlation between the measured SF and its drivers, evidenced through coefficients of determination ($R^2$) of 0.82, 0.99 and 0.92 for the relationships between SF and short-grass reference evapotranspiration ($ET_o$), stem area and stomatal conductance, respectively. The measured and simulated SF varied from 0.82–1.29 and 0.71–1.19 mm tree$^{-1}$ day$^{-1}$ (model parameterization), as well as from 0.77–3.54 and 1.10–3.10 mm tree$^{-1}$ day$^{-1}$ (model validation). Despite the slight discrepancies between measured and predicted SF values during model performance evaluation, an acceptable agreement was achieved through root mean square errors (RMSEs) of 0.32 and 0.37 mm day$^{-1}$ and model efficiencies (Efs) of 0.93 and 0.88, for model parameterization and validation, respectively. The current study showed that the canopy conductance T model has the potential to accurately predict Moringa T and contribute to optimizing irrigation water management.

## 1. Introduction

Moringa (*Moringa oleifera* Lam.) is a nutrient-dense and multipurpose drought-tolerant crop that can grow under both rainfed and irrigated conditions (Dalal et al., 2021). However, the species is confronted with the challenges of low commercial potential due to limited exploitation, and the scanty research thereof, largely with regard to the water use (WU) and eco-physiological characteristics (dos Santos et al., 2017). Understanding Moringa WU for optimum irrigation scheduling can be improved by implementing plant-based water monitoring methods. Accurate plant measurements, including the use of sap flow (SF) sensors, enable the assessment of the effects of biotic and abiotic stresses on transpiration (T), but can at the same time contribute to the calibration of models such as the canopy conductance model described by Wheeler et al. (2023).

Several methods can be used for a direct assessment of crop WU, including but not limited to soil water balance measurements, field lysimeters, eddy covariance (EC), residual energy balance (EB), Bowen ratio-energy balance (BR), sap flow (SF), and plant chambers (Anapalli et al., 2018). Except for the SF method, other approaches are less dynamic and timing-susceptible, costly, labour-intensive, and tailored for research ends (Grime et al., 1995; Ismanov et al., 2022). To date, the stem SF technique has become the unique approach to be adopted for regular real-time measurements of plant T and improved water management at large (Kumar et al., 2022). Further, it is well documented that monitoring the ecosystem SF in agro-forestry is critical for estimating the dynamics of plant WU and T, as well as plant vigour and responses to water-related stressors (Ozcelik et al., 2022; West et al., 2023). Several SF measurement methods have been developed by many authors (Li et al., 2022; Zeng et al., 2022). However, the stem heat

* Corresponding author.
*E-mail address:* martin.steyn@up.ac.za (J.M. Steyn).
[1] Present address: Agricultural Research Council, Natural Resources and Engineering, Pretoria, South Africa.

https://doi.org/10.1016/j.agwat.2024.109127
Received 10 June 2024; Received in revised form 22 September 2024; Accepted 20 October 2024
Available online 30 October 2024

balance (SHB) method developed by Sakuratani (1981) is widely used and emerged somewhat more advantageous than others, partly due to the fact that it is real-time, non-intrusive and calibration-free.

Regardless of the method or the scale chosen for measurements, the daily plant SF is affected by diverse factors such as tree characteristics, environmental variables or a combination of multiple factors. The major tree traits which guide the pattern of plant SF include the trunk internal temperature, the stem water potential, the angle of tree deviations from the vertical, and the normalized difference vegetation index (NDVI) (Safargalieva et al., 2021). Other physiological (e.g., canopy width and leaf area index (LAI)) (Guerrieri et al., 2019) or agronomic (e.g., plant density) factors (Hassler et al., 2018; Suarez et al., 2021) were also classified in this category. The most contributing environmental variables driving SF include soil water potential (Cao et al., 2020; Korakaki and Fotelli, 2021), soil texture (Hassler et al., 2018), solar radiation and vapor pressure deficit (VPD) (Korakaki and Fotelli, 2021; Safargalieva et al., 2021; Rissanen et al., 2024; Wan et al., 2024), photosynthetically active radiation (PAR) (Cao et al., 2020; Suarez et al., 2021), air temperature (Cao et al., 2020), surface terrain inclination (Kume et al., 2016; Schoppach et al., 2021) and slope orientation (Hassler et al., 2018).

SF measurements from individual stems can practically be upscaled to the entire tree and stand (Duan et al., 2017), although caution must be exercised while selecting the adequate scaling-up methods (Wang et al., 2022). Past experience proved that these methods were highly variable in spite of the characteristics considered (effective and actual leaf area (LA), leaf area index (LAI), canopy coverage, basal area, sapwood area) (Poyatos et al., 2016). The study by Wang et al. (2019) indicated that the stem-scale SF in caragana korshinsk shrubs (*Caragana korshinskii*) presented a positive linear correlation with the stem base diameter, stem length, primary branch numbers in the stem, and estimated stem biomass. Although the variables considered for the study could be used in the conversion of SF between different scales, the findings of Fan et al. (2022a, 2022b) maintained that the SF velocity has obvious radial variability in trunk sections. Moreover, the validity of upscaling outcomes significantly depended on the scalar multipliers of the independent variables between the trees and the stand. For appropriate irrigation scheduling, there is a need to determine evapotranspiration (ET) precisely, which requires the input of local data that are not always available. Furthermore, some techniques such as large drainage lysimeters and EC equipment cannot be installed in all cropped areas, whereas their long-term maintenance is problematic (Anapalli et al., 2018). In this regard, state-of-the-art agricultural system models are cheap, viable, and widely accepted tools for developing location-specific crop ET data for irrigation scheduling and crop-ET response functions to accurately determine crop water needs (McNider et al., 2015).

Efficient water management can be improved through a determination of the effect of different factors on SF. However, although the nexus of SF and its drivers is well-documented, no model has yet been adopted for the prediction of SF change of several tree species, including Moringa (Mashamaite et al., 2021). Additionally, parametric models (e.g., regression models) which are usually developed to characterize the relationships between SF and its driving factors were not only found to be relatively few (Zabihi et al., 2023), but also not pertinent to Moringa. Therefore, this study aimed at estimating T of Moringa by measuring and modelling the SF of intact main stems using an improved heat balance technique. The specific objectives of this study were to: (1) measure branch and stem SF of irrigated mature Moringa trees, (2) upscale the measured SF from stem- to plant-level, (3) identify the major morpho-eco-physiological parameters that affect daily SF, and (4) parameterize and validate a canopy conductance model to predict daily T of Moringa.

## 2. Materials and methods

### 2.1. Description of the study site

The study was conducted on a 9-year-old, drip-irrigated Moringa stand (*Moringa oleifera* Lam., cultivar PKM-1) and covered the growing periods of two consecutive seasons (2021–2022 - Season 1 and 2022–2023 - Season 2) at the Roodeplaat Experimental Farm of the Agricultural Research Council–Vegetable, Industrial and Medicinal Plants (ARC–VIMP) (25°35'S, 28°21'E, 1164 m.a.s.l.) (Fig. 1). During the 2021–2022 growing season, the study was carried out in autumn (May 2022) and involved two representative trees of 20–30 % canopy coverage (CC). In the 2022–2023 growing season the study was implemented from mid-summer (February) when the canopy cover was an average of 60–70 % until winter (June) when the canopy cover declined to 10–20 %. The study area lies within a semi-arid climatic region, with an average annual rainfall of 650 mm, predominantly during the summer season (mainly October–March) (Mabhaudhi et al., 2014). Average daily air temperatures ($T_a$) fluctuate from 8–34 °C (summer) and 4–23 °C (winter), whereas January and July are the hottest and coldest months, respectively (Mokgehle et al., 2022). The end of autumn is characterized by little or no rainfall, while frost may occur from the beginning of May (van Rooyen et al., 1986). In line with the United States Department of Agriculture (USDA) taxonomic system, the soil texture of the study site is classified as sandy clay loam (containing on average 65 % sand, 8 % silt and 27 % clay), while the respective slope and soil depth are 0.5–1 % and > 1.2 m, with an average bulk density of 1200 kg $m^{-3}$.

### 2.2. Crop management

The experimental trees were grass-mulched (Fig. 2a) for soil water conservation and were spaced at 1 m x 1 m (intra-row x inter-row), giving a total planting density of 10000 plants $ha^{-1}$. The trees were fertilized with plant-derived compost (C:N ratio = 30:1) for organic soil amendment, which was applied once at the rate of 150 ton $ha^{-1}$ in the beginning of each growing season (October to November). Soil water content of the tree root zone (up to 90 cm) was monitored using 10-HS automated capacitance soil water sensors installed at 30-cm depth intervals in the soil profile. These points of the root zone where most of the roots were concentrated coincided with a close proximity to the emitters/drippers. The sensors were connected to an EM50 datalogger (Decagon Devices Inc.) and readings were taken on an hourly basis. Irrigation water application was conducted by an automatic irrigation controller (Rainbird ESP-TM2, Azusa, California, USA) through the regulation of a solenoid valve connected to a pressure-compensated drip irrigation system. The system consisted of one drip line for each row of Moringa trees and one dripper per tree, and operated at a pressure of 100–150 kPa to deliver water at a rate of 4 L $h^{-1}$. The soil water content was maintained close to field capacity (0.36 $m^3$ $m^{-3}$) to ensure well-watered conditions. One hour (4 mm) of irrigation was typically applied once every second to third day, depending on climatic conditions and the occurrence of rainfall events.

The trees were harvested at 45-day intervals using a stripping method (plucking the leaves from the trees, with only a few leaves remaining on top of the tree for continuous photosynthesis). The cutback of Moringa trees occurred at the end of the growth season, viz. after frost occurrence and when the stems were dry and the trees were completely leafless.

### 2.3. Environmental parameters

Key environmental parameters were recorded on an hourly and daily basis. These parameters included air temperature ($T_a$ - minimum ($T_{min}$), average ($T_{ave}$) and maximum ($T_{max}$)) and solar radiation (SR), which were monitored using a Tinytag TV-4500 datalogger (Gemini Data

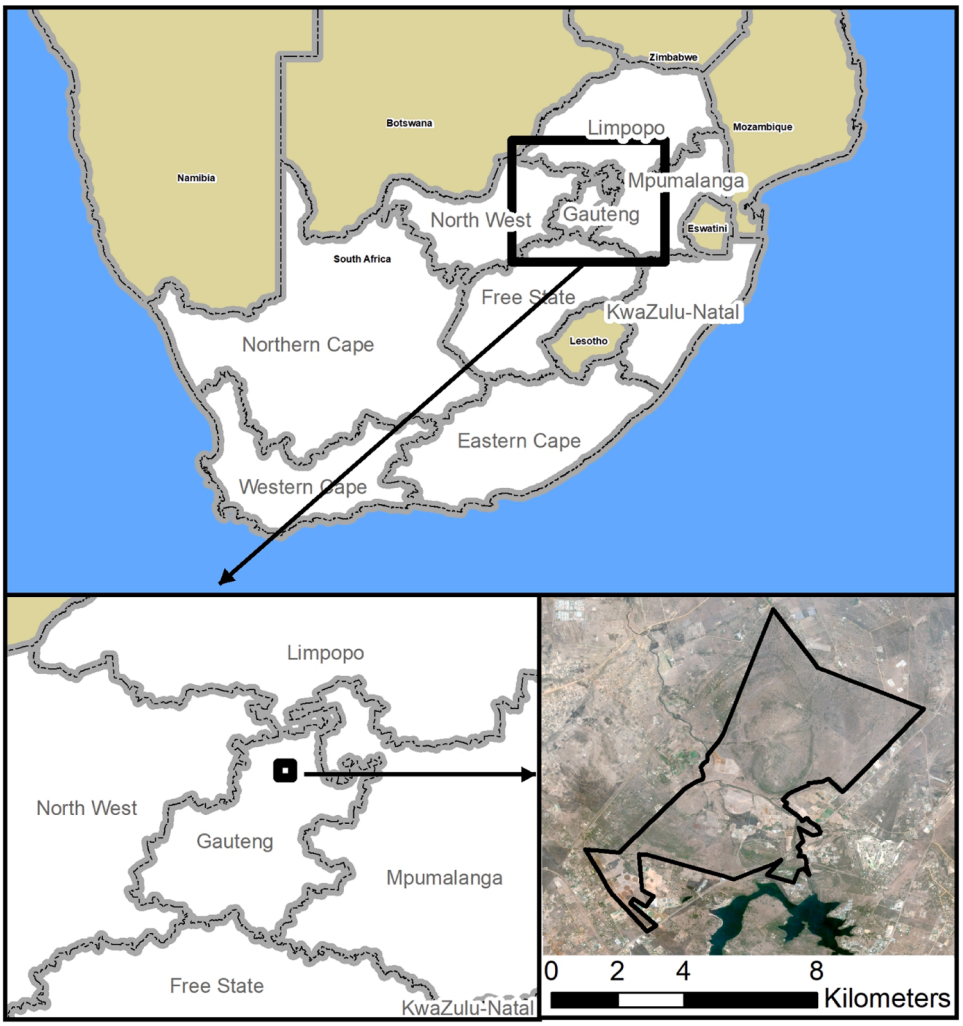


**Fig. 1.** Map to indicate location of the Moringa trial site at Roodeplaat, Gaueng Province, South Africa.

Loggers, UK) smart sensor and an apogee pyranometer (Apogee Instruments Inc., Logan, UT, USA), respectively. The values of wind speed ($u_2$) and rainfall were obtained from the nearest automatic weather station installed and managed by the Agricultural Research Council–Natural Resources and Engineering (ARC–NRE). The short-grass reference evapotranspiration ($ET_o$) during the experimental period was computed on hourly (Eq. 1) and daily (Eq. 2) timesteps using the Penman-Monteith equation.

$$ET_o = \frac{0.408\Delta(R_n - G) + r\frac{37}{T_{hr}+273}u_2(e^o(T_{hr}) - e_a)}{\Delta + r(1 + 0.34u_2)} \quad (1)$$

$$ET_o = \frac{0.408\Delta(R_n - G) + r\frac{900}{T+273}u_2(e_s - e_a)}{\Delta + r(1 + 0.34u_2)} \quad (2)$$

where $ET_o$ is the reference evapotranspiration (mm $hr^{-1}$ or mm $day^{-1}$), $R_n$ is the net radiation at the crop surface (MJ $m^{-2}$ $hr^{-1}$ or MJ $m^{-2}$ $day^{-1}$), G is the soil heat flux density (MJ $m^{-2}$ $hr^{-1}$ or MJ $m^{-2}$ $day^{-1}$), which is usually considered negligible (Allen et al., 1998), $T_{hr}$ (hourly) and T (daily) are the mean air temperatures at 2.0 m height (°C), $u_2$ is the wind speed at 2.0 m height (m $s^{-1}$), $e^\circ$ ($T_h$) is the saturation vapour pressure at air temperature $T_{hr}$ (kPa), $e_s$ is the saturation vapour pressure ($kP_a$), $e_a$ is the actual vapour pressure (kPa), ($e_s$−$e_a$) is the saturation vapour pressure deficit (kPa), $e^\circ$ ($T_{hr}$) − $e_a$ is the saturation vapour pressure deficit at air temperature $T_{hr}$ (kPa), Δ is the saturation slope of the vapour pressure-temperature curve (kPa $°C^{-1}$), γ is the psychrometric constant (0.0673 (hourly), 0.066 (daily) kPa $°C^{-1}$), whereas 37 (hourly), 900 (daily) and 0.408 are coefficients that account for the conversion from energy levels to equivalent water amounts.

### 2.4. Morpho-physiological parameters

Main morpho-physiological parameters were monitored on an hourly and daily basis for 8–9 days, from 9h00 to 16h00 on the fully developed third leaves from the top of selected branches. These parameters involved leaf stomatal conductance ($g_s$) and chlorophyll fluorescence using an LI-600 LiCor system (Li-Cor, Inc., Lincoln, Nebraska, USA), PAR and leaf area index (LAI) using an AccuPAR LP-80 ceptometer (Decagon Devices Inc., Pullman, WA, USA), as well as leaf chlorophyll content (SPAD readings) using a Minolta SPAD-502 chlorophyll meter (Minolta Camera Co. Ltd, Japan). Chlorophyll fluorescence denotes the maximum quantum efficiency of PSII and it is the ratio of variable chlorophyll fluorescence (Fv) to maximum chlorophyll fluorescence (Fm). The fractional interception of PAR was calculated as in Eq. 3. In addition, morphological parameters such as the number of stems per tree, stem diameter (D), stem area (SA), and leaf area (LA) were also recorded (Table 1).

$$FI_{PAR} = 1 - \frac{PAR_i}{PAR_o} \quad (3)$$

where $FI_{PAR}$ is the intercepted PAR, $PAR_i$ is the amount of PAR mleasured at ground level under the tree canopy, and $PAR_o$ is the amount of

**Fig. 2.** (a) Thirteen-year-old grass-mulched Moringa stand with (b) EXO-Skin sap flow sensors installed on the stems.

incoming global PAR.

### 2.5. Sap flow measurements

Sap flow (SF) sensors of varying sizes (10–25 mm diameter) were installed on main stems and branches to determine the T of two representative trees (Tree 1 and Tree 2), selected based on a survey study conducted across the entire Moringa stand (Fig. 2b). The survey study was carried out prior to the SF experiment, around November to December of each growing season, when the Moringa stand was fully established. The characteristics of the trees and sensors used for SF measurement are shown in Table 1.

The stem heat balance (SHB) approach (EXO-Skin sap flow sensors, Dynamax Inc., Houston, USA) was adopted for the current study (Fig. 2b), and the details of the theory, as well as the field installation procedures for this SF system can be found in Dynamax Inc. manuals and were reported by researchers such as Dong and Hansen (2023). Briefly, once the representative trees were identified, the stem diameter corresponding to that of a selected sensor was assessed using a Vernier caliper. In order to secure a firm contact between the stem and the sensor, the surface of the stem section to be equipped with the sensor was lightly smoothed using sandpaper. Adequate protective natural oil (canola) was then sprayed onto the stem section to prevent the sensor from sticking to the stem. Prior to wrapping the sensor around the stem, the canola oil was also applied to the sensor internal side to avert sticking and corrosion. The insulation, protection, as well as binding of the sensor to the stem were consolidated using Velcro straps, towels, insulation tubes, wax paper and aluminum foil. Micro-Tec G4 silicone grease was also applied while connecting the sap flow sensors to the pigtails of a datalogger (CR1000X datalogger (Campbell Sci. Inc., Logan, UT, USA) with datalogger support software (LoggerNet)). SF sensors were installed in suitable positions (Table 1) on the stems to prevent interferences such as water from rain and irrigation, as well as thermal effects through incident solar radiation. The tree SF was measured and recorded every 15 min by the datalogger. SF rate was calculated using Eq. 4 (Shackel et al., 1992):

$$F = \frac{Pin - Qv - Qr}{CpxdT} \tag{4}$$

where F is the instantaneous sap flow rate (SFR) (g $hr^{-1}$); Pin is the heat input (W); Qr is the radial heat dissipation (W); Qv is the vertical thermal conductivity (W); Cp is the specific heat of water (4.186 J $g^{-1}$ $^{o}C^{-1}$); and dT is the temperature differential between the two vertical thermocouples (°C).

The measured SF data were converted into hourly and daily timescales, whereas the recorded stem/branch SF was summed up to determine the total tree SF. In addition, the Microsoft Excel Software (version 2016) was used for model building and running of simulations. Daily tree T was calculated as the accumulation of the hourly SF, whereas stand T was calculated using a weighted average T determined based on the representativeness of stem diameters obtained through a survey study conducted prior to SF measurements. All the SF calculations were conducted per unit area. The measured SF was used to develop regression models linked to the various microclimatic and morpho-eco-physiological parameters. Likewise, the daily SF was used to estimate the transpiration coefficient ($K_t$), determined as the ratio of crop T to $ET_o$ on condition that the root zone held adequate soil water content for optimum T (Yang et al., 2022). If the amount of water that is stored in

**Table 1**
Characteristics of the trees and sensors used for sap flow measurements during the experimental period.

| Tree no. | Stem/ branch no. | Tree traits | | Sensor details | | |
|---|---|---|---|---|---|---|
| | | [a]SD (cm) | [b]LA ($m^2$) | Sensor no. | Sensor D (mm) | [c]Sensor position (cm) |
| **2021–2022 (Season 1)** | | | | | | |
| Tree 1 | Stem 1 | 1.6 | 0.3948 | 4 | 16 | 70 |
| | Stem 2 | 2.6 | 0.2916 | 6 | 25 | 70 |
| | Branch 1 | 1.0 | 0.176 | 1 | 10 | 125 |
| | Branch 2 | 0.9 | 0.193 | 2 | 10 | 120 |
| Tree 2 | Stem 1 | 2.5 | 0.369 | 7 | 25 | 70 |
| | Stem 2 | 2.0 | 0.5838 | 8 | 25 | 70 |
| | Stem 3 | 1.7 | 0.4963 | 5 | 16 | 70 |
| | Stem 4 | 1.1 | 0.320 | 3 | 10 | 122 |
| **2022–23 (Season 2)** | | | | | | |
| Tree 1 | Branch 1 | 1.0 | 0.3300 | 1 | 10 | 70 |
| | Branch 2 | 1.0 | 0.2115 | 2 | 10 | 85 |
| | Stem 1 | 1.5 | 0.3374 | 5 | 16 | 40 |
| | Stem 2 | 2.7 | 0.2354 | 8 | 25 | 22 |
| | Stem 3 | 2.3 | 0.3848 | 9 | 25 | 25 |
| | Stem 4 | 3.2 | 0.3483 | 10 | 25 | 40 |
| | Stem 5 | 2.3 | 0.3010 | 11 | 25 | 40 |
| | Stem 6 | 1.2 | 0.3739 | 4 | 10 | 75 |
| Tree 2 | Stem 7 | 1.5 | 0.3921 | 6 | 16 | 25 |
| | Stem 8 | 3.5 | 0.2208 | 12 | 25 | 40 |
| | Stem 9 | 1.0 | 0.4103 | 3 | 10 | 70 |
| | Stem 10 | 3.2 | 0.3739 | 13 | 25 | 25 |
| | Stem 11 | 2.4 | 0.3119 | 14 | 25 | 40 |
| | Stem 12 | 2.1 | 0.1333 | 15 | 25 | 25 |

[a] SD stands for stem diameter.
[b] LA stands for leaf area.
[c] Sensor position is the height from the soil surface.

the plant tissues is assumed negligible, the crop T can be linked to the daily SF. As a result, $K_t$ can be calculated as the ratio of plant SF to $ET_o$: $K_t = SF/ET_o$, where $K_t$ is the transpiration coefficient; SF is the daily SF amount (mm $day^{-1}$); and $ET_o$ is the daily short-grass reference evapotranspiration (mm $day^{-1}$), as defined in Eq. 2. The daily $K_t$ data was then used to calculate weekly mean $K_t$ values. Only the SF data recorded under ideal weather conditions (especially rainless days) contributed to the computation of $K_t$.

### 2.6. Parameterization of the canopy conductance transpiration model

The measured SF was also used to fit a canopy conductance ($g_c$) driven T model (Villalobos et al., 2013). The approach used to predict $g_c$ with the model of Villalobos et al. (2013) is based on the concept that canopy assimilation is proportional to radiation interception. Estimates of $g_c$ are subsequently included in the derivation of crop parameters (a (μE $mol^{-1}$) and b (μE $mol^{-1}$ $kPa^{-1}$)) through the linear regression of ($FI_{PAR}$*SR)/$g_c$ against VPD, which are then used for direct estimates of daily T (mm $day^{-1}$) using Eq. 5:

$$T = 37.08 \quad x \quad 10^{-3} \frac{FI_{PAR} \quad SR}{a + bVPD} \; x \; \frac{VPD}{P_a} \tag{5}$$

where $FI_{PAR}$ is the fraction of photosynthetically active radiation intercepted by the canopy (dimensionless), SR is the total daily solar radiation (J $m^{-2}$ $day^{-1}$), $P_a$ is the daily average atmospheric pressure (kPa), VPD is the daily average vapour pressure deficit (kPa), the coefficient $37.08 \times 10^{-3}$ incorporates the conversion of units for Joules of solar radiation to mol quanta and from mol to kg of $H_2O$, while *a* and *b* are the intercept and slope of the linear function relating ($FI_{PAR}$*SR)/$g_c$ to VPD. The daily $FI_{PAR}$ was determined using a well parameterized and validated radiation interception model as in Ibraimo (2018). Diurnal bulk canopy conductance ($g_c$, mm $day^{-1}$) was computed through an inversion of the evaporation equation (Orgaz et al., 2007; Villalobos et al., 2013), using the measured SF data. Fig. 3 depicts the complete flowchart of the research methodology used, including model development and testing.

### 2.7. Performance of the canopy conductance model

Field data collected from Season 1 was used to calibrate the canopy conductance model, whereas model validation was performed on the independent data set of Season 2. The model performance was evaluated against several statistical parameters, including the coefficient of determination ($R^2$), the mean absolute error (MAE), the mean absolute percent deviation (MAPD), the root mean square error (RMSE), the coefficient of efficiency (Ef) (Nash and Sutcliffe, 1970), the Willmott index of agreement (d) (Willmott and Matsuura, 2005), and the coefficient of residual mass (CRM) (Eitzinger et al., 2004) (Table 2).

In Table 2, n is the number of observations, $S_i$ and $O_i$ are the simulated and observed values for the corresponding parameter, respectively; while $\bar{O}$ is the mean of the observed variable. The respective scopes of variation of MAE (%) and MAPD (%), RMSE (mm $day^{-1}$), and CRM are from 0–100, 0–+∞ and -∞–+∞. RMSE assumes the same unit as the variable under observation. The model goodness of fit increases as MAE, MAPD, RMSE and CRM values approach 0. The values of $R^2$, d and Ef range from 0 to 1, and the closer their values are to 1, the better the agreement (strength) between the simulated and measured values. The acceptable levels for most of these metrics can be seen in Table 2, except for RMSE and CRM. An RMSE value of less than half the standard deviation of the measured data was reported to be appropriate (Moriasi et al., 2007). For the latter, positive values indicate that the model has a tendency to underestimate the data while negative values designate that the model tends to overestimate the observations (Hosaini et al., 2009).

### 2.8. Ethical considerations

Since this was a quantitative study conducted on a research farm, there were no particular ethical considerations to be made.

## 3. Results

### 3.1. Environmental characteristics

The major environmental variables are summarized in Fig. 4 and varied according to time of the day or the year. For Season 1, the study took place in autumn and the amplitude of variations was small due to the fact that the weather conditions at the study site were mostly partly cloudy, interspersed with a few clear days, especially towards the end of the study period. The lowest $T_{min}$ was at the end of measurements on May 31st 2022, when the first frost occurred. On this day, the lowest $T_{min}$ was −0.57, and was accompanied with decreased $T_{max}$, VPD, SR and $ET_o$, increased wind velocity, while the response of SWC was inconsistent, although relatively higher than in the previous period (data not shown). No irrigation water was supplied since it was not required. The soil temperatures equally declined during that period (data not shown). For this study period, the ranges of $T_{min}$, $T_{max}$, VPD, SR, $ET_o$ and wind velocity were: −0.57–15.66 °C, 18.71–41.29 °C, 0.61–1.64 kPa, 5.68–30.45 MJ $m^{-2}$ $day^{-1}$, 1.07–4.23 mm, and 0.36–1.40 m $s^{-1}$, respectively.

The rainfall amount was 22 mm from two rain events, which took place towards the end of the rainy season. The trend in the variation of environmental conditions during the autumn of Season 2 was similar to that for Season 1. The ranges for the respective variables were: 1.60–16.27 °C, 18.11–35.15 °C, 0.03–2.49 kPa, 4.34–25.15 MJ $m^{-2}$ $s^{-1}$, 0.88–5.60 mm, and 0.31–1.83 m $s^{-1}$. The observed soil temperatures were also affected by the prevailing microclimatic conditions (not shown). The study during Season 2 also covered 20 days of summer (February) and 19 days of winter (June). Except for the winter when wind velocity was the highest, the highest values generally occurred in

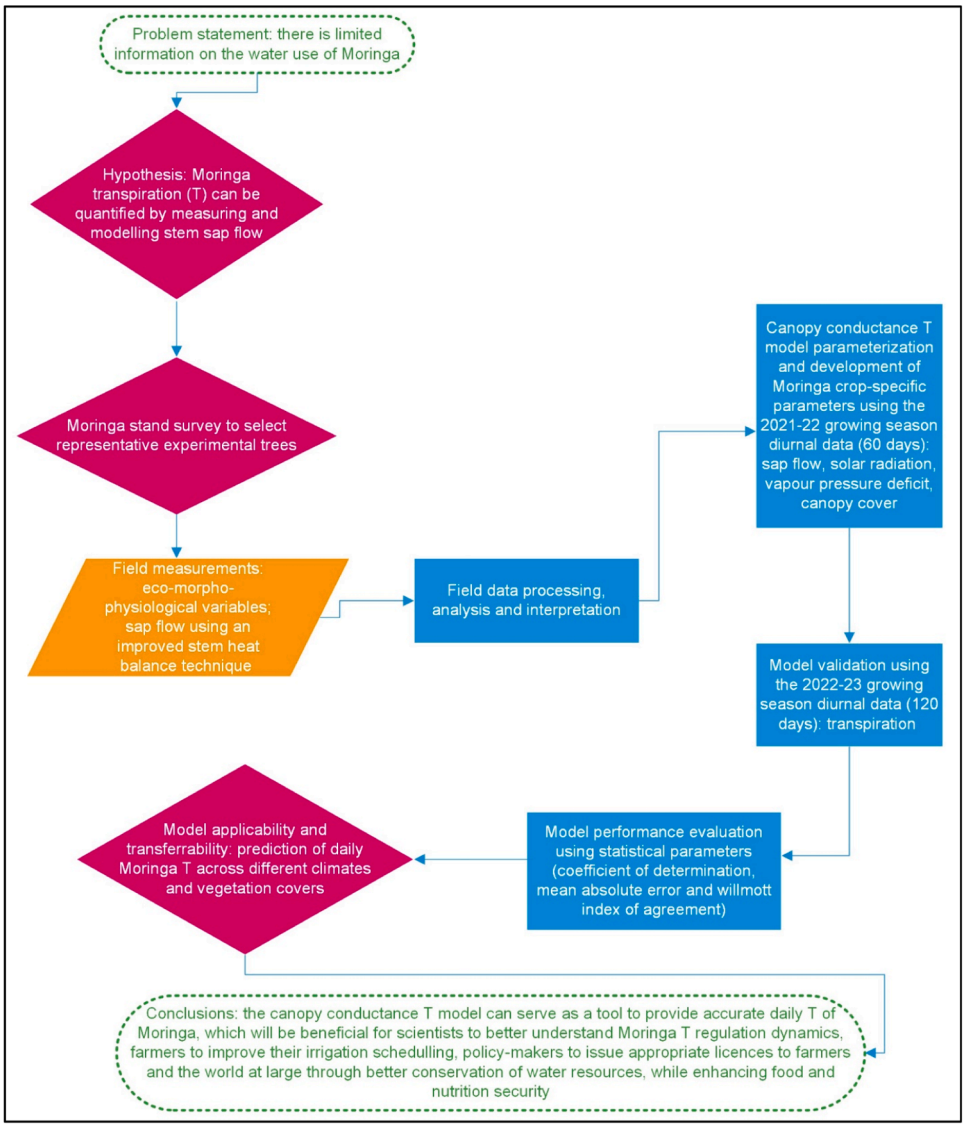


**Fig. 3.** A schematic diagram illustrating the conceptualization of the research study on the measurement and modelling of Moringa transpiration.

**Table 2**
Model performance assessment criteria (Nash and Sutcliffe, 1970; Eitzinger et al., 2004; Singh et al., 2005; Willmott and Matsuura, 2005).

| Parameters | Formula | Eq. | Strength | Range (optimum) |
|---|---|---|---|---|
| Coefficient of determination ($R^2$) | $\frac{\sum S_i O_i - \sum S_i + \sum O_i}{\sqrt{\sum S_i^2 - (\sum S_i)^2}\ \sqrt{\sum O_i^2 - (\sum O_i)^2}}$ | 6 | > 0.80 | 0–1 (1.00) |
| Mean absolute error (MAE) (%) | $\frac{1}{n}\sum_{i=1}^{n} \lvert S_i - O_i \rvert$ | 7 | < 20 | 0–100 (0.00) |
| Mean absolute percent deviation (MAPD) (%) | $\frac{1}{n}\sum_{i=1}^{n} \left\lvert \frac{O_i - S_i}{O_i} \right\rvert$ | 8 | < 25 | 0–100 (0.00) |
| Root mean square error (RMSE) (mm $day^{-1}$) | $\sqrt{\frac{1}{n}\sum_{i=1}^{n} (S_i - O_i)^2}$ | 9 | – | 0–+∞ (0.00) |
| Willmott index of agreement (d) | $1 - \frac{\sum_{i=1}^{n} (S_i - O_i)^2}{\sum_{i=1}^{n} (\lvert S_i - \bar{O} \rvert + \lvert O_i - \bar{O} \rvert)^2}$ | 10 | > 0.80 | 0–1 (1.00) |
| Coefficient of efficiency (Ef) | $1 - \frac{\sum_{i=1}^{n} (S_i - O_i)^2}{\sum_{i=1}^{n} (O_i - \bar{O})^2}$ | 11 | > 0.75 | -∞–1 (1.00) |
| Coefficient of residual mass (CRM) | $\frac{\sum_{i=1}^{n} O_i - \sum_{i=1}^{n} S_i}{\sum_{1=1}^{n} O_i}$ | 12 | – | -∞–+∞ (0.00) |

summer and the lowest in winter. The SWC in Season 2 ranged from 0.326–0.374 $m^3\ m^{-3}$ (Fig. 5) and was influenced by the amounts of rainfall and the irrigation water applied. Season 2 received 33 rain events, which generated 440 mm of rainwater, varying from 1–78 mm each, while the total cumulative $ET_o$ for the same period was 430.4 mm. Water was supplied and withheld intermittently, depending on the sporadic rainfall events. Therefore, the applied irrigation amounts fluctuated between 2.1–4.7 mm, while the range of the combination of

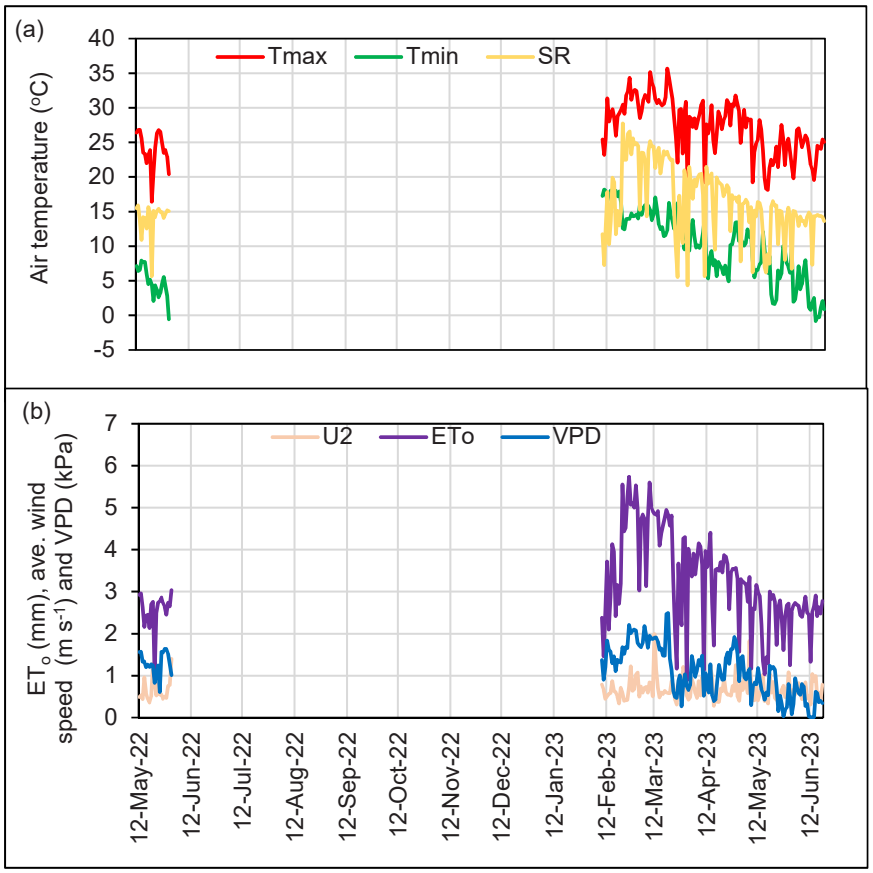


**Fig. 4.** Microclimatic conditions during the sap flow trial for Seasons 1 and 2 at the study site: (a) maximum temperature ($T_{max}$), minimum temperature ($T_{min}$) and solar radiation (SR), and (b) short-grass reference evapotranspiration ($ET_o$), average wind speed and vapour pressure deficit (VPD).

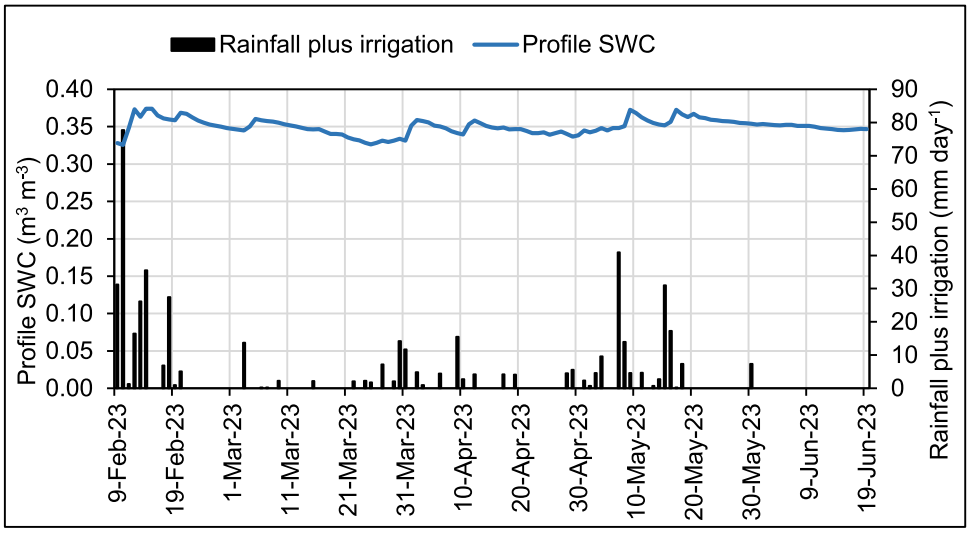


**Fig. 5.** Profile soil water content (SWC), rainfall and irrigation for Season 2 at the study site.

rainfall and irrigation was similar to that for rainfall. The aggregate rainfall and irrigation water amounted to 488.5 mm.

### 3.2. Morpho-physiological characteristics

In response to the microclimatic conditions and the time of the day or day of the year, the eco-physiological variables progressed as in Fig. 6. During Season 1 (Fig. 6 left), although the weather conditions at the study site were mostly partly cloudy, with only a few clear days, there were dissimilarities between the two experimental trees in the different physiological variables. In general, the values of the physiological variables were higher for Tree 2 (e.g., stomatal conductance: 163 mmol $m^{-2}$ $s^{-1}$) than in Tree 1 (e.g., stomatal conductance: 140 mmol $m^{-2}$ $s^{-1}$). From Table 1 it is evident that Tree 2 was morphologically larger than Tree 1. As in the case of the microclimatic factors, the fluctuations of the eco-physiological characteristics were

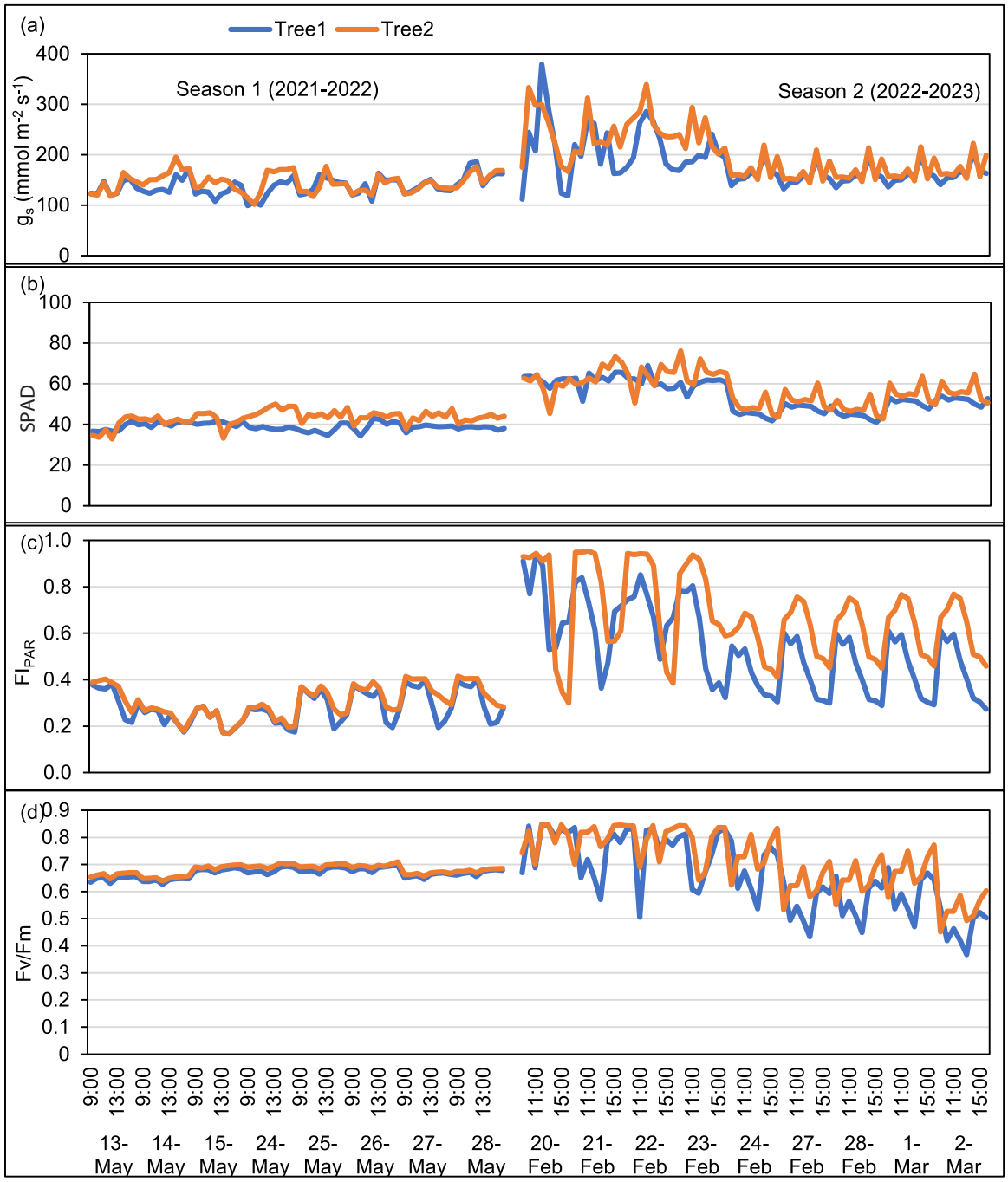


**Fig. 6.** Variability of Moringa leaf physiological variables: (a) stomatal conductance ($g_s$), (b) SPAD, (c) fractional interception of photosynthetically active radiation ($FI_{PAR}$) and (d) chlorophyll fluorescence (Fv/Fm), for selected days in Seasons 1 (2021–2022) and 2 (2022–2023) at the study site..

also narrow during the study period. Similar to stomatal conductance (Fig. 6a), SPAD values (b), $FI_{PAR}$ (c) and chlorophyll fluorescence (d), for Tree 1 were also lower than Tree 2. The respective ranges for Season 1 were: 127–160 and 134–163 mmol m$^{-2}$ s$^{-1}$, 37–41 and 39–47, 0.228–0.317 and 0.229–0.364, as well as 0.642–0.686 and 0.650–0.696. This can mainly be attributed to the larger size of Tree 2 (four stems of D between 1.0 and 2.5 cm and canopy LA of 2.1 m$^2$) compared to Tree 1 (two stems of D between 1.6 and 2.6 cm and canopy LA of 0.69 m$^2$). Stomatal conductance values generally increased under conditions of high atmospheric evaporative demand, particularly at high daily SR, $T_{max}$ and VPD.

For Season 2, the prevalence of Tree 2 over Tree 1 was maintained due to their allometric traits, and the respective ranges for the different physiological variables (Fig. 6a–d right) where the respective variables ranged as follows: 154–221 and 164–267 mmol m$^{-2}$ s$^{-1}$, 44–62 and 48–66, 0.419–0.734 and 0.559–0.794, and 0.467–0.793 and 0.533–0.803. The differences between the values of Season 1 and Season 2 were partly due to temporal variations in climate, as the physiological variables were measured in autumn for Season 1, while in Season 2 the measurements took place during summer. Additionally, the start of data collection in Season 2 (20–24 February) was marked with relatively lower $T_{min}$ and wind velocity, accompanied with relatively higher $T_{max}$, SR, VPD and overall atmospheric evaporative demand, which is represented by $ET_o$ (Fig. 7). Consequantely, most of the Moringa physiological responses ($g_s$, SPAD, $FI_{PAR}$, Fv/Fm and others such as SF (Section 3.3)) increased markedly.

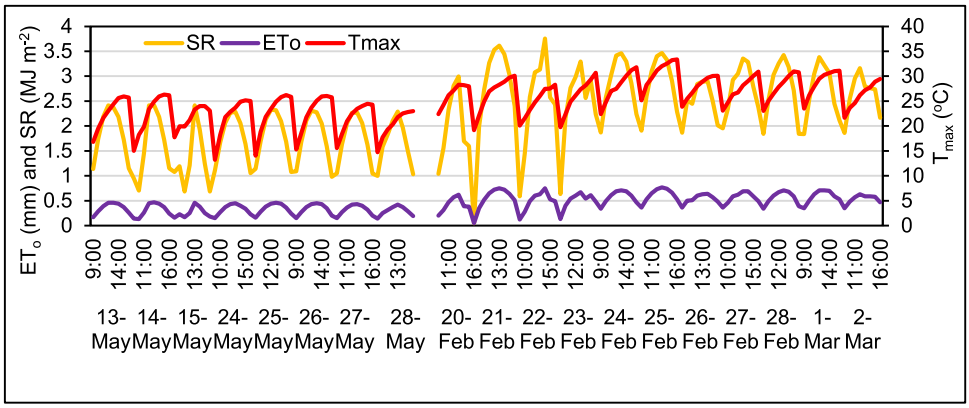


**Fig. 7.** Hourly atmospheric evaporative demand, which is represented by $ET_o$, as well as maximum temperatures ($T_{max}$) and solar radiation (SR) for selected days in seasons 1 (2021–2022) and 2 (2022–2023) at the study site.

### 3.3. Sap flow characteristics and transpiration coefficients

The results of the hourly and daily SF are given in Figs. 8 and 9, respectively. For Season 1 (Fig. 8a), the complete hourly data set is presented, while only part of the hourly data recorded in the autumn of Season 2 is plotted. All the daily data recorded during both seasons are illustrated in Fig. 9. According to observations, the cyclic trend of SF indicates peaks in the mornings and troughs at night, with Tree 1 always having lower SF (including short peaks) than Tree 2. This can mainly be attributed to the morpho-physiological traits of these trees, as described in Table 1. In terms of Season 1 (Figs. 8a and 9a, CC: 30 %), the highest hourly (0.640 L tree$^{-1}$ hr$^{-1}$) and daily (1.624 L tree$^{-1}$ day$^{-1}$) SF values were recorded for Tree 2 on a relatively warm clear day, while Tree 1 peaked (0.344 L tree$^{-1}$ hr$^{-1}$ and 1.059 L tree$^{-1}$ day$^{-1}$) on another relatively mild, clear day. This crest of Tree 1 represents 46 % (hourly) and 35 % (daily) lower values, compared to Tree 2. The ranges in SF values for Tree 1 were 0.002–0.344 (hourly) and 0.379–1.059 (daily) L, while for Tree 2 it varied from 0.001–0.640 (hourly) and 0.965–1.624 (daily) L.

The higher SF of Tree 2 compared to Tree 1 persisted throughout Season 2. This season was divided into three different periods: summer (last 20 days of February) (Fig. 9b, CC: 70 %), autumn (March–May) (Fig. 9c, CC: 90 %) and winter (first 19 days of June) (Fig. 9d, CC: 40 %). The hourly SF for Tree 2 ranged from 0.000–2.550 (summer), 0.000–1.637 (autumn), and 0.000–0.483 (winter) L tree$^{-1}$. The corresponding daily values extended from 3.769–15.817, 1.854–11.503, and 0.962–2.728 L tree$^{-1}$. For Tree 1, the hourly SF varied from 0.000 – 0.366 (summer), 0.000–0.294 (autumn), and 0.000–0.019 (winter) L tree$^{-1}$. On a daily basis, the SF of Tree 1 fluctuated from 0.237–2.263, 0.089–1.856, and 0.008–0.061 L tree$^{-1}$. In the autumn season, except for the hourly SF of Tree 1 in Season 1 when SF was higher than that of Season 2, the highest hourly (Tree 2) and daily (Tree 1 and Tree 2) SF values generally occurred in Season 2. For the entire duration of Season 2, the highest SF was recorded in summer and the lowest in winter. For instance, the respective highest daily SF values for Tree 2 were 16, 12 and 3 L tree$^{-1}$. The decreasing trend was modulated by the environmental weather conditions such as lower $ET_o$ (Fig. 8c). Furthermore, the hourly and daily SF changed from branch to branch, while the SF of the combined branches was always lower than that of the main stem.

In addition, Fig. 8 also indicates that the diurnal SF of both seasons experienced some days with multiple peaks, especially in Season 2 (Fig. 8). Season 1 only covered around three weeks in autumn. The nocturnal SF was negligible, and so were the peaks thereof. The multiple peaks were linked to unstable climatic conditions such as cloudy or rainy days. Compared to the monomodal peaks with standard periodicity, the possible features of the multimodal peaks were: aberration in periodicity, differences in magnitude, bimodal peaks with an event in the morning and another in the afternoon, trimodal peaks (not shown) with one occurrence in the morning and 2 in the afternoon, or vice versa. In general, the bimodal peaks were characterised by great and small levels in the morning and afternoon, respectively. However, both peaks could occur during the same period (morning or afternoon), and the peak magnitude is imposed by the intensity of the prevailing weather conditions, especially SR. The trimodal peaks are equally regulated by the SF driving forces. Another observation is that the SF of the two study trees could peak at the same or separate times without a clear indication of which one was reaching the highest point first.

In terms of $K_t$, which was calculated to guide future Moringa WU estimation and irrigation scheduling, the average $K_t$ for Season 1 was 0.293, whereas the average weekly $K_t$ values for Season 2 are illustrated in Fig. 10a. It is worth noting that the crop canopy coverage for Season 1 was around 30 %, while that of Season 2 developed according to temporal and management circumstances. The leaves of the SF study trees were stripped at harvest after a 45-day regrowth period. The SF study period was divided into three shorter periods according to the time of Moringa leaf harvest. These were the period of Moringa regrowth from the second harvest to the third (average $K_t$: 0.616), from the third to the fourth harvest (average $K_t$: 0.536), and the end (after the fourth harvest) (average $K_t$: 0.225). The $K_t$ and SF curves (Fig. 10a) followed the same patterns, which show three-lobed graphs, and aligned with the pattern of SF. Each lobe is related to a Moringa regrowth cycle (after leaf stripping) and characterized by an increasing stage, a summit and a decreasing stage. The first lobe is the highest and the third the lowest. The strength of the first lobe was influenced by suitable summer conditions, which are reflected in relatively high $ET_o$ values (Fig. 10a) in response to the high levels of other environmental variables (Fig. 10b). The increase is also due to the vigorous crop regrowth with favourable environmental conditions experienced after the second harvest. Both curves reached their maximum on the fourth week after harvest and 25th week of Season 2, then started to decline due to the moderate autumn weather conditions and the third crop harvest. The peak weekly $K_t$ and SF values were 0.819 and 3.23 L tree$^{-1}$ day$^{-1}$, respectively, which corresponded to an average $ET_o$ of 3.94 mm day$^{-1}$. The end of the graph shows lowest values as the winter onset jeopardized the growth potential of a warm-weather crop such as Moringa. It is noteworthy to state that the study period for Season 2 spanned from the end of summer, full autumn and the start of winter, as mentioned in Section 3.1. Further, in general all environmental variables were decreasing steadily (Fig. 10a, b) in conformity with the seasonal fluctuations.

### 3.4. Response of sap flow to microclimatic and morpho-eco-physiological conditions

The SF of Moringa trees was influenced by microclimatic and

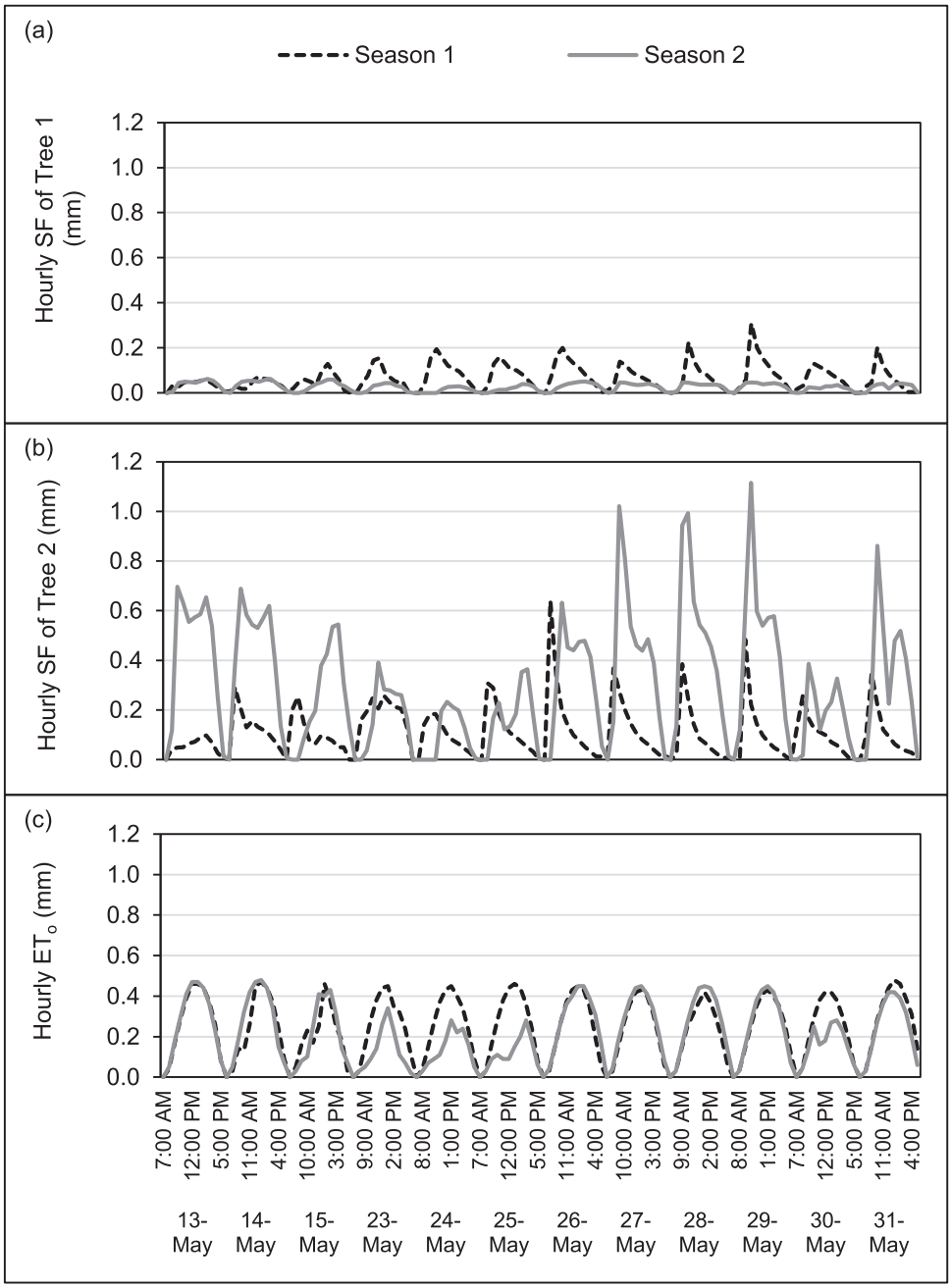


**Fig. 8.** Hourly Moringa sap flow (SF) at the study site: (a) for Tree 1 and (b) for Tree 2 in Seasons 1 (2022) and 2 (2023), as well as (c) short-grass reference evapootransporation ($ET_o$).

morpho-eco-physiological conditions, as shown in Fig. 11 (hourly SF), Table 3 (daily SF), and Fig. 10 (weekly SF, Section 3.3). To test the hourly response of SF to microclimatic factors, two days with either clear sky or partly cloudy weather characteristics were selected in summer, autumn and winter of Season 2. The periodic progress of SF (Fig. 11a–f) was driven by microclimatic factors, especially SR. $T_{ave}$ and $ET_o$ were second and third most important, respectively, while wind velocity was the least controlling factor. The shape and peaks of SF adhered to those of SR and $ET_o$ perfectly, including multiple peaks. It is also obvious that the brightness of the day alone was not a major factor affecting SF, as the interference of the time of the year (the season) cannot be underrated. For example, periods of clear skies displayed outstandingly disimilar SF and SR values in summer (Fig. 11a), autumn (Fig. 11c) and winter (Fig. 11e). The respective SF (L tree$^{-1}$ h$^{-1}$) for Tree 1 and Tree 2 were: 0.366 and 2.550, 0.225 and 1.637, and 0.019 and 0.483. The corresponding hourly SR values (MJ m$^{-2}$) were: 3.41, 2.92, and 1.55 respectively. Except for the first SR value, which was the peak of the day and occurred nearly at the same time as the peak SF, the second SR value lagged behind the peak of the day (2.93 MJ m$^{-2}$ h$^{-1}$), while the last SR value preceded the peak of the day (2.22 MJ m$^{-2}$ h$^{-1}$). In addition, the daily records showed strong positive correlations between the measured SF and the related microclimatic and morpho-eco-physiological drivers ($R^2$ up to 0.99). The exception was observed for $T_{min}$ and the wind velocity, which resulted in poor correlations, with $R^2$ equalling to 0.50 and 0.40, respectively. The $T_{min}$ is reached at night when SF is nearly zero. The marked response of SF to $ET_o$, SR, $T_{max}$ and VPD was reflected in $R^2$ values of 0.82, 0.77, 0.74 and 0.72, respectively. Additionally, SF was reported to preserve a strong dependence on morpho-physiological conditions. During the present study, LA, SA, stomatal conductance and SPAD values correlated well with SF and gave

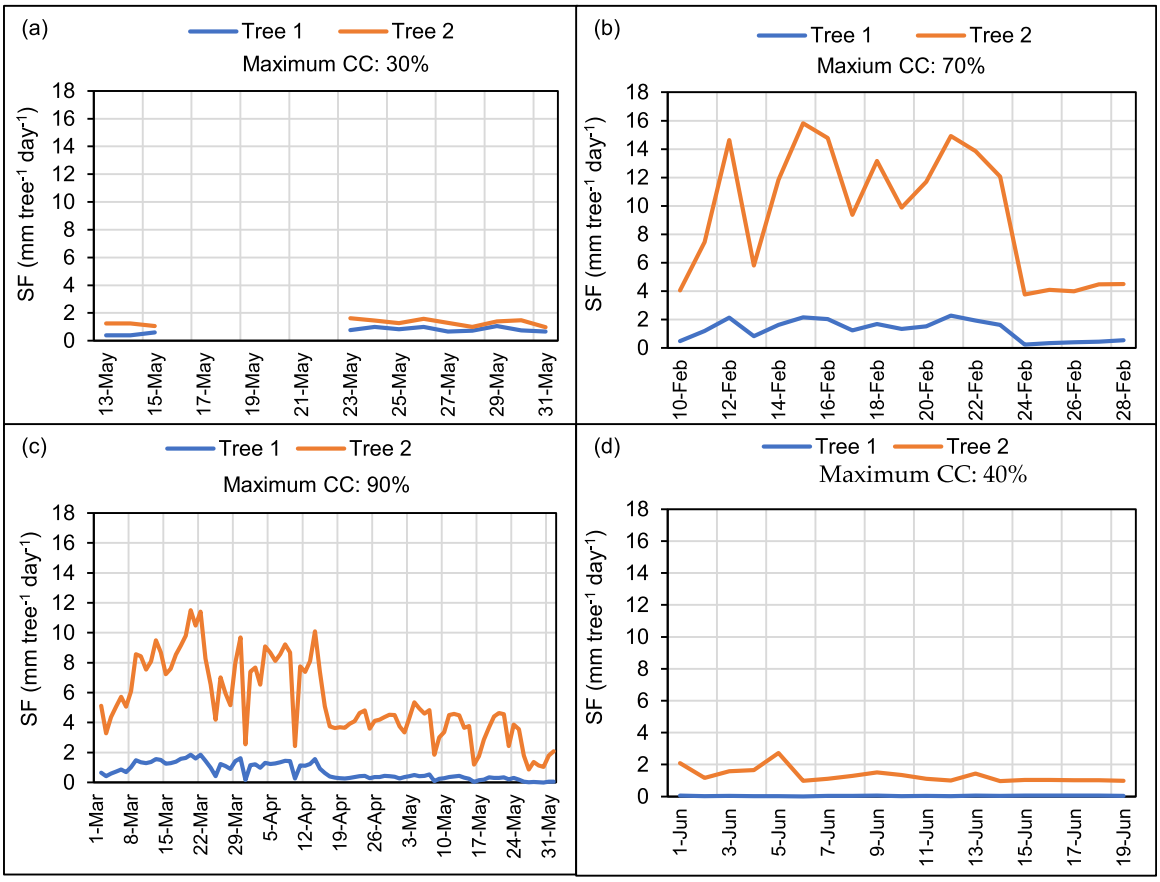


**Fig. 9.** Daily Moringa sap flow (SF) and canopy cover (CC) during: (a) autumn of Season 1 and (b), (c) and (d) summer, autumn and winter of Season 2, respectively.

$R^2$ values of 0.85, 0.99, 0.92 and 0.97, respectively. With respective $R^2$ of 0.80 and 0.72, chlorophyll fluorescence and $FI_{PAR}$ were also positively correlated with SF, although to a lesser extent than other morpho-physiological factors. SA, stomatal conductance and SPAD values became the leading morphological and physiological drivers of SF compared to LA, Fv/Fm and $FI_{PAR}$. Moreover, the present study substantiated that LA and SA can be reliable upscaling factors for SF.

### 3.5. Modelling of Moringa daily transpiration

The results on the parameterization and validation of the canopy conductance T model are shown in Fig. 12 and Table 4. Although the measured SF was, in general, slightly higher than the simulated SF (model parameterization) or vice versa (model validation), both phases reflected evidence of a good agreement between the measured and simulated T. In terms of parameterization, the model performance according to the selected metrics was as follows: $R^2$ = 0.88, MAPD = 1.22 %, MAE = 2.70 %, RMSE = 0.32 mm $day^{-1}$, d = 0.94, Ef = 0.93 and CRM = 0.04. The respective stats for model validation were 0.76, 10.24 %, 0.15 %, 0.37 mm $day^{-1}$, 0.82, 0.88, and −0.05. For model parameterization, the averages of the measured and simulated T (derived from SF) varied from 0.82 – 1.29 and 0.71–1.19 mm $tree^{-1}$ $day^{-1}$, respectively. During model validation, the respective ranges were: 0.77–3.54 and 1.10–3.10 mm $tree^{-1}$ $day^{-1}$. In addition, during the model parameterization, the coefficients a and b (Table 5) derived for the Moringa trees were 675 μE $mol^{-1}$ and 2430 μE $mol^{-1}$ $kPa^{-1}$, respectively. Afterwards, the empirical coefficient $D_o$ (a reflection of the effect of VPD on stomatal closure) was determined as the ratio a/b and amounted to 0.28 (Table 5). The size of the canopy, especially when integrated into the inherent microclimatic and other morpho-physiological conditions, plays a pivotal role in driving crop T. Accordingly, the composite factor of $FI_{PAR}$, SR and $g_c$ was regressed against VPD and a positive correlation was achieved, with an $R^2$ of 0.81 for the two trees combined.

## 4. Discussion

### 4.1. Sap flow characteristics and transpiration coefficients

The curves of the hourly and daily SF presented a periodicity of peaks in the mornings and troughs at night. In the cases of Fan et al. (2022a, 2022b) and Kumar et al. (2023), the respective peaks of the SF of golden pear and secondary tropical montane forests also occurred in the mornings. However, Dong and Hansen (2023) reported that the SF of potato peaked at mid-day, while for Pradiko et al. (2022), the SF of oil palm increased gradually until the peak after midday. The extent of the peaks also varied from season to season, from tree to tree and from timescale to timescale, mostly guided by the prevailing weather conditions, as was reported by Duan et al. (2017). Likewise, most of the SF occurred during daytime and only a small portion was nocturnal. This was confirmed by Li et al. (2024), while investigating the SF rate of poplar, willow and locust trees mostly due to elevated relative humidity, as well as diminished solar radiation and air temperature. Subsequently, tree SF resumed in the mornings as a result of increases in solar radiation and air temperature, with declining relative humidity. Fisher et al. (2007) and Sun et al. (2021) postulated that the percentage of the nocturnal SF depends on many factors, especially the climate, crop type, and growth stage.

The present study showed that the hourly and daily SF of the combined tree branches were always lower than that of the SF of the main stem, while the branches also differed due to their respective positions on the main stem. This corroborates the findings reported by Burgess

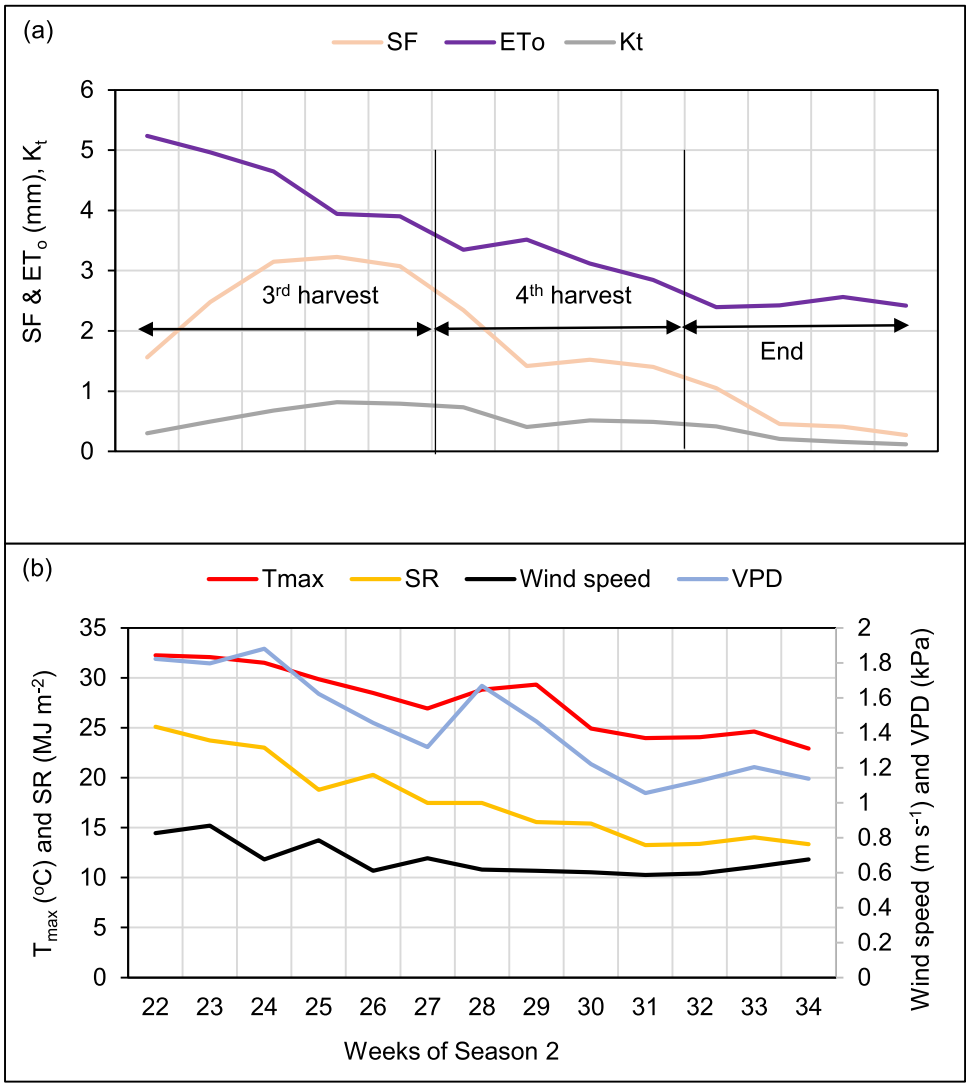


**Fig. 10.** Weekly Moringa transpiration coefficient ($K_t$), sap flow (SF) and short-grass reference evapotranspiration ($ET_o$) (a), as well as other related atmospheric variables (b) during Season 2, at the study site.

and Dawson (2008) and Roddy and Dawson (2013). Roddy and Dawson (2013) also established SF imbalance between branches or between specific branches and their main stems, mostly due to various factors affecting the root-to-leaf continuum such as positional variability, capacitance (storage) and hydraulic resistance.

In the current study, Moringa $K_t$ was shown to be affected by iterative leaf stripping–leaf regrowth management practices and $K_t$ changed according to the prevailing environmental and phenological conditions. $K_t$ is used with $ET_o$ in the determination of the crop WU, and it depends on the crop type and development stage. As expected, $K_t$ followed the tree growth curve, with low initial values at the start of leaf production, and then consistently developed to the highest level at peak canopy cover, prior to declining again to a low level at the end of the growth cycle. Yang et al. (2022) also reported varying SF-related $K_t$ values in greenhouse tomato. However, the average $K_t$ found for the different seasons and growth cycles of the present study were lower than those reported by dos Santos et al. (2017), which fluctuated between 0.73 and 1.73 for the different phenological stages of Moringa. The current study revealed mean weekly $K_t$ values for Moringa ranging from 0.225–0.616, although the larger tree (Tree 2) had an average weekly $K_t$ of 0.819 in the summer of Season 2. This discrepancy can partly be assigned to the different biotic and abiotic factors affecting growth and SF at the different study sites.

### *4.2. Response of sap flow to microclimatic and morpho-eco-physiological conditions*

This study aimed to characterize Moringa SF and to delineate its major driving forces. The findings revealed that the variation of the eco-physiological variables were partly regulated by major environmental variables which, in turn, depended on time of the day or the year. The main environmental driving variables were $ET_o$, SR, $T_{max}$ and VPD. An analysis of these environmental factors also shed light on the specific correlations between the selected variables (data not shown). The literature maintains a strong interconnection among the SF driving factors and the complexity thereof (Zhao et al., 2017; Wu et al., 2023), including their independence or synergy (Safargalieva et al., 2021; Wu et al., 2023). Further, the study by Wei et al. (2017) concluded that the four different phases (the period of increasing flow, peak flow, period of declining flow, and stable flow level) of daily SF were functions of seasonal, physiological and environmental factors.

Although SR and $T_{max}$ (with $R^2$ of 0.77 and 0.74, respectively) were not the leading environmental drivers during the current study, it is well-documented that a strong correlation links SF and these factors (Zhang et al., 2015; Guerrieri et al., 2019; Wang et al., 2019), and to a great extent, to PAR (Roddy and Dawson, 2013; Zhang et al., 2015; Zhou et al., 2015; Wang et al., 2019; Wei et al., 2017; He et al., 2023). Similar

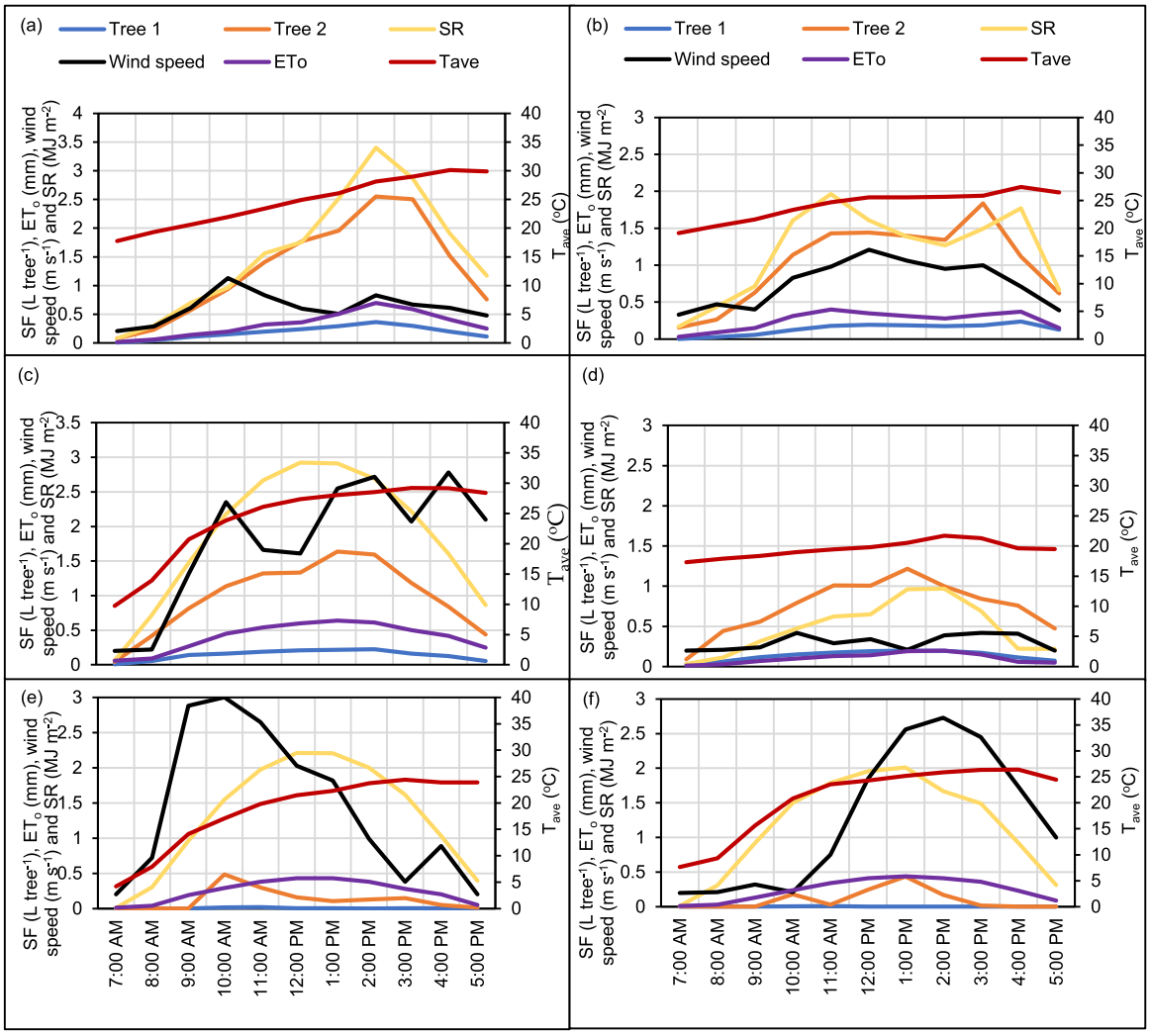


**Fig. 11.** Moringa hourly sap flow (SF) and its environmental drivers viz. short-grass reference evapotranspiration ($ET_o$), wind speed, solar radiation (SR) and average air temperature ($T_{ave}$) on selected days of Season 2 at the study site: clear-sky days (a, c, e for summer, autumn and winter, respectively), as well as partly cloudy days (b, d and f for the respective periods).

to the findings of the present study, Wheeler et al. (2023) established that $ET_o$ as the major environmental driver regulating the SF of jujube. Moreover, SF rates mostly slow down as $T_{max}$ and VPD decrease, and RH increases (Hentschel et al., 2015). This was also confirmed in the current study, particularly for $T_{max}$, but also for other atmospheric variables such as SR, VPD, and $ET_o$. SR and VPD were also documented to correlate strongly with the SF movement in Euphrates poplars (*Popular euphratica* L.) (Wan et al., 2024) and diverse urban trees (Rissanen et al., 2024).

Additionally, this study proved that the impact of environmental variables is reflected in both the seasonal and daily variability of SF. The literature also referred to the seasonality and daily progression of SF, including the multiplicity of peaks due to unfavourable conditions such as extreme environmental conditions (Zhang et al., 2015; Kumar et al., 2023). The SF recorded during the current study also showed multiple peaks on some days, particularly with occasional overcast conditions.

Furthermore, SF was reported to preserve a strong dependence on plant morpho-physiological conditions (Guerrieri et al., 2019; Fan et al., 2022a, 2022b). The study by Wang et al. (2019) indicated that the stem-scale SF in caragana korshinsk shrubs (*Caragana korshinskii*) presented a positive linear correlation with the stem base diameter, stem length, primary branch numbers in the stem, and estimated stem biomass. Likewise, physiological characteristics such as effective and actual LA, LAI, canopy coverage, basal area or sapwood area were reported to play a crucial role in the plant life cycle, including SF dynamics (Poyatos et al., 2016). The response of SF to stomatal closure enables the assessment of water stress, water loss, and T rate, specifically in woody plants (Noun et al., 2022). During the present study, LA, SA, stomatal conductance, and chlorophyll fluorescence correlated well with SF, with $R^2$ values of 0.72–0.99. In terms of morpho-physiological parameters, SF was primarily driven by SPAD, SA and stomatal conductance. The eco-physiological characteristics are also partly a function of different environmental factors, for example, through wind and air temperature that can interfere with the tree canopy foliage, especially nocturnal stomatal conductance (Fan et al., 2022a, 2022b; McAusland et al., 2023).

### 4.3. Modelling of Moringa daily transpiration

This study also intended to parameterize and validate a canopy conductance T model for irrigation management and the findings revealed a good agreement between measured and simulated SF. According to the literature, the canopy conductance model is used in a simplified format to avoid the complex model parameterization process (Alam et al., 2021). The model may tend to over- or underestimate net T due to its intrinsic functionality and simplicity (Irmak et al., 2008; Ibraimo, 2018). Nonetheless, the present study and literature have proven that a reasonable agreement could be established between

**Table 3**
Relationships between Moringa daily transpiration and microclimatic or morpho-physiological variables.

| Variables | | Equations | $R^2$ |
|---|---|---|---|
| Microclimatic | Maximum temperatures (°C) | #$y = 0.0067x^2 - 0.0959x - 0.713$ | 0.742 |
| | Minimum temperatures (°C) | $y = 0.0032x^2 + 0.1173x + 0.4931$ | 0.496 |
| | Vapour pressure deficit (kPa) | $y = 0.5895x + 0.2058$ | 0.717 |
| | Wind velocity (m $s^{-1}$) | $y = -0.3363x + 1.2605$ | 0.403 |
| | Solar radiation (MJ $m^{-2}$ $day^{-1}$) | $y = 0.0029x^2 + 0.119x - 1.208$ | 0.766 |
| | Reference evapotranspiration (mm) | $y = 0.0399x^2 + 1.2798x - 2.0804$ | 0.821 |
| Morphological | Leaf area ($m^2$ $m^{-2}$) | $y = 0.5824x + 0.691$ | 0.851 |
| | Stem area ($cm^2$) | $y = 9.8056x - 2.1504$ | 0.985 |
| Physiological | Stomatal conductance (mmol $m^{-2}$ $s^{-1}$) | $y = 0.0002x^2 - 0.0402x + 2.1359$ | 0.920 |
| | SPAD readings | $y = 0.0104x^2 - 0.903x + 20.579$ | 0.967 |
| | §Fv/Fm | $y = 130.99x^2 - 159.13x + 49.098$ | 0.803 |
| | *$FI_{PAR}$ | $y = 22.353x^2 - 13.471 + 3.0703$ | 0.721 |

# y stands for dependent variable (transpiration) and x stands for independent variables. § Fv stands for variable chlorophyll fluorescence and Fm stands for maximum chlorophyll fluorescence. * $FI_{PAR}$ stands for the fractional interception of the photosynthetically active radiation.

measured and simulated T (Ibraimo, 2018). This is due to the fact that the model enables the assessment of stomatal T through the conductance or resistance of the plant canopy. Furthermore, the canopy conductance model in question was also conceived to account for the dynamics of canopy conductance through the alterations in the coefficients a and b derived from the correlative influence of the atmospheric $CO_2$ concentration and the subsequent changes in radiation use efficiency (RUE) (Villalobos et al., 2013; Alam et al., 2021).

Although the Moringa crop-specific coefficients derived in the present study can not be supported by literature, mostly due to the fact that the crop remains under-researched, Table 5 shows a comparison of Moringa and other crops such as nuts (Ibraimo, 2018) and citrus trees (Vahrmeijer and Taylor, 2018). The empirical coefficient $D_o$ (a reflection of the effect of VPD on stomatal closure) for Moringa (0.28) was lower than that of pecan (0.40), but higher than the outcomes for macadamia (0.18) and orange (0.23). This coefficient (ratio a/b) is characteristic to crops and measures the inverse proportionality between VPD and the canopy conductance condition; an increase in $D_o$ usually indicates high canopy conductance with a decrease in VPD (Leuning, 1995). Villalobos et al. (2013) reaffirmed an immense irregularity that characterizes the robust coupling between the canopy of fruit trees (like Moringa) and the atmospheric conditions. In other words, ET (especially T) of these trees is more dependent on the canopy conductance and VPD, instead of solar radiation, which is the main determinant of T in annual or short crops. Therefore, the Moringa coefficients generated from the T conductance model in the present study imply to some extent that the crop is performing better in water storage and drought resistance than pecan. However, the same logic (Table 5) holds that the crop is outclassed by orange and macadamia in this regard. The results from the present study suggest that the evaluated canopy conductance T model has the potential to be an effective tool to predict Moringa T for optimal irrigation water management, which should be beneficial to various stakeholders such as irrigation scientists, engineers and decision-makers.

**Table 5**
Regressions of the ratio of radiation interception and canopy conductance versus vapour pressure deficit (VPD). The intercept (a) and slope (b) of the linear regression equations are also shown, including the empirical coefficient Do, calculated as the ratio a/b, which reflects the effect of VPD to the status of stomatal closure.

| Tree crops | a (μE $mol^{-1}$) | b (μE $mol^{-1}$ $kPa^{-1}$) | $D_o$ | $R^2$ | References |
|---|---|---|---|---|---|
| Moringa | 675 | 2430 | 0.2778 | 0.8095 | Current study |
| Pecan | 1029 | 2600 | 0.3958 | 0.8400 | Ibraimo (2018) |
| Macadamia | 650 | 3700 | 0.1757 | 0.8200 | Ibraimo (2018) |
| Orange | 850 | 3631 | 0.2340 | 0.6900 | Vahrmeijer and Taylor (2018) |

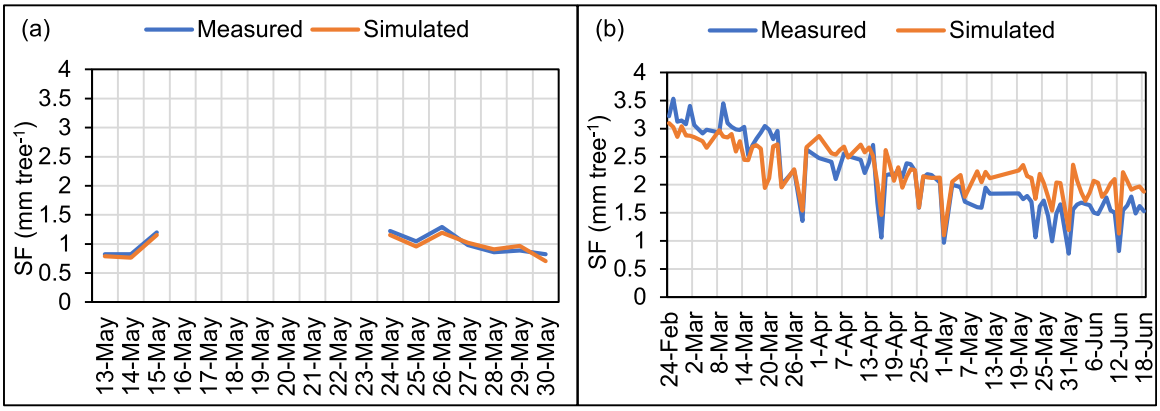


**Fig. 12.** A comparison between measured and simulated transpiration (derived from sap flow (SF)) for: (a) Season 1 - model parameterization and (b) Season 2 - model validation.

**Table 4**
Performance assessment criteria for the canopy conductance T model.

| Phases | $R^2$ | MAE (%) | MAPD (%) | RMSE (mm $day^{-1}$) | d | Ef | CRM |
|---|---|---|---|---|---|---|---|
| Parameterisation | 0.883 | 2.696 | 1.224 | 0.320 | 0.939 | 0.930 | 0.036 |
| Validation | 0.758 | 0.153 | 10.236 | 0.370 | 0.819 | 0.884 | −0.053 |

## 5. Conclusions

Moringa tree T was highly influenced by tree size (determined by the number of stems per tree, SA, as well as LA). The major microclimatic influencing variables of SF were $ET_o$, followed by SR and $T_{max}$, LA, SA, stomatal conductance and SPAD values were the morpho-physiological variables with best positive correlations with SF. Moringa mean crop coefficient ($K_t$) was 0.293 in Season 1 (autumn), while $K_t$ values in Season 2 varied according to the specific growing period: 0.62 (summer), 0.54 (autumn), and 0.23 (winter). The measured and simulated SF for the two seasons varied from 0.82–1.29 and 0.71–1.19 mm tree$^{-1}$ day$^{-1}$ (model parameterization; Season 1), and from 0.20–4.24 and 0.51–3.42 mm tree$^{-1}$ day$^{-1}$ (model validation; Season 2). During model parameterization, the intercept (coefficient a) of the canopy transpiration model was 675 μE mol$^{-1}$ and the slope (coefficient b) was 2430 μE mol$^{-1}$ kPa$^{-1}$. Despite the slight underestimation of the predicted versus the recorded SF, an acceptable agreement was detected through a root mean square error (RMSE) and a model efficiency (Ef) of 0.32 mm day$^{-1}$ and 0.93, respectively. During model validation, the simulated SF values were slightly higher than the recorded amounts, but a reasonable match characterized them through an RMSE of 0.37 mm day$^{-1}$ and an Ef of 0.88. It is also noteworthy that this model is prone to poor performance (inaccurate results) if operated under the weather conditions of low solar radiation (partly cloudy or overcast days). However, under cloudless weather conditions it should be a useful tool to estimate Moringa WU in order to facilitate irrigation scheduling for optimum productivity. Moreover, although the empirical and semi-empirical models proposed in this study should be useful to help estimate Moringa T for improved irrigation management, more mechanistic models may provide better results.

The study addressed the challenges raised in the introduction through the following: (1) the species is confronted with the challenges of low commercial potential due to limited exploitation, and the scanty research thereof, largely with regard to the WU and eco-physiological characteristics. This study quantified for the first time Moringa transpiration and provided a better understanding of its environmental regulation in relation to morpho-eco-physiological drivers; (2) the lack of an accurate method to upscale Moringa sap flow from branch to plant level was addressed. This study tested and identified appropriate morpho-physiological parameters to upscale Moringa sap flow from branch/stem to plant level; and (3) tree water use is highly variable, depending on environmental conditions and tree canopy size amongst other variables. This study parameterized and evaluated a mechanistic physiological model to predict Moringa T more accurately across a range of climates and stand vegetation covers.

In addition, the present study established that Moringa SF is a function of multiple variables such as environmental, morpho-ecophysiological, seasonal, growing period and growth-stage. The measured SF data served as the basis for the parameterization and validation of the canopy conductance T model, which performed well in both phases of the study. Since the current study developed crop specific parameters for Moringa and successfully tested model performance using an independent growing season dataset, the usefulness and transferability thereof was proven. The model should therefore be applicable to other locations where it can make a positive socio-economic impact on Moringa production.

## CRediT authorship contribution statement

**Joachim Martin Steyn:** Writing – review & editing, Visualization, Validation, Supervision, Software, Resources, Project administration, Methodology, Investigation, Funding acquisition, Formal analysis, Conceptualization. **Christian Phillipus du Plooy:** Writing – review & editing, Visualization, Validation, Software, Resources, Project administration, Methodology, Investigation, Funding acquisition, Formal analysis, Conceptualization. **Ambroise Ndayakunze:** Writing – review & editing, Writing – original draft, Methodology, Data curation, Conceptualization. **Nadia Alcina Araya:** Writing – review & editing, Visualization, Validation, Supervision, Software, Resources, Project administration, Methodology, Investigation, Funding acquisition, Formal analysis, Conceptualization.

## Funding

This project was funded by the Water Research Commission (Project No C2020/2021-00484) of the Republic of South Africa.

## Declaration of Competing Interest

The authors declare the following financial interests/personal relationships which may be considered as potential competing interests: Ambroise Ndayakunze reports financial support was provided by Water Research Commission. Ambroise Ndayakunze reports financial support was provided by University of Pretoria. All other authors declare that they have no known competing financial interests or personal relationships that could have appeared to influence the work reported in this paper.

## Acknowledgments

The authors would like to thank the Water Research Commission (Project No C2020/2021-00484) for funding this research, the Agricultural Research Council for managing the project, as well as the University of Pretoria for student capacity building. Our gratitude is also extended to Mr Harold Weepener, from the ARC – Natural Resources and Engineering, Geoinformatics division, for creating the study site map.

## Data availability

Data will be made available on request.

## References

Alam, M.S., Lamb, D.W., Warwick, N.W.M., 2021. A canopy transpiration model based on scaling up stomatal conductance and radiation interception as affected by leaf area index. Water 13, 252. https://doi.org/10.3390/w13030252.

Allen, R.G., Pereira, L.S., Raes, D., Smith, M., 1998. Crop evapotranspiration: guidelines for computing crop water requirements. FAO Irrigation and Drainage Paper 56. FAO, Rome, Italy.

Anapalli, S.S., Green, R.G., Reddy, K.N., Marek, G., 2018. Application of an energy balance method for estimating evapotranspiration in cropping systems. Agric. Water Manag. 204. https://doi.org/10.1016/j.agwat.2018.04.005.

Burgess, S.S.O., Dawson, T.E., 2008. Using branch and basal trunk sap flow measurements to estimate whole-plant water capacitance: a caution. Plant Soil 305, 5–13.

Cao, Q., Li, J., Xiao, H., Cao, Y., Xin, Z., Yang, B., Liu, T., Yuan, M., 2020. Sap flow of *Amorpha fruticosa*: implications of water use strategy in a semiarid system with secondary salinization. Sci. Rep. 10, 13504.

Dalal, N.R., Bhalekar, M.N., Ranpise, S.A., Dalal, S.R., 2021. Irrigation water management on growth, flowering and yield of drumstick (*Moringa oleifera* Lamk.) cv. Bhagya. J. Pharmacogn. Phytochem. 10 (2), 749–752.

Dong, Y., Hansen, H., 2023. Comparison of methods for estimating crop water use: sap flow, FAO-56 Penman-Monteith, and weather parameters. Agric. Sci. 14, 617–628. https://doi.org/10.4236/as.2023.145041.

Duan, L.M., Lv, Y., Yan, X., Liu, T.X., Wang, X.X., 2017. Upscaling stem to community-level transpiration for two sand-fixing plants: *Salix gordejevii* and *Caragana microphylla*. Water 9, 361. https://doi.org/10.3390/w9050361.

Eitzinger, J., Trnka, M., Hosch, J., Zalud, Z., Dubrovsky, M., 2004. Comparison of CERES, WOFOST and SWAP models in simulating soil water content during growing season under different soil conditions. Ecol. Model. 171, 223–246.

Fan, B., Liu, Z., Xiong, K., Li, Y., Li, K., Yu, X., 2022. Influence of environmental factors on the sap flow activity of the golden pear in the growth period of Karst Area in Southern China. Water 14, 1707. https://doi.org/10.3390/w14111707.

Fan, Y., Lv, Z., Qin, B., Yang, J., Ren, K., Liu, Q., Jiang, F., Zhang, W., Ma, S., Ma, C., Huang, Z., 2022. Night warming at the vegetative stage improves pre-anthesis photosynthesis and plant productivity involved in grain yield of winter wheat. Plant Physiol. Biochem. 186, 19–30. https://doi.org/10.1016/j.plaphy.2022.06.015.

Fisher, J.B., Baldocchi, D.D., Misson, L., Dawson, T.E., Goldstein, A.H., 2007. What the towers don't see at night: nocturnal sap flow in trees and shrubs at two AmeriFlux sites in California. Tree Physiol. 27, 597–610.

Grime, V.L., Morison, J.I.L., Simmonds, L.P., 1995. Including the heat storage term in sap flow measurements with the stem heat balance method. Agric. For. Meteorol. 74, 1–25. https://doi.org/10.1016/0168-1923(94)02187-O.
Guerrieri, R., Belmecheri, S., Ollinger, S.V., Asbjornsen, H., Jennings, K., Xiao, J., Stocker, B.D., Martin, M., Hollinger, D.Y., Bracho-Garrillo, R., et al., 2019. Disentangling the role of photosynthesis and stomatal conductance on rising forest water-use efficiency. Proc. Natl. Acad. Sci. 116, 16909–16914.
Hassler, S.K., Weiler, M., Blume, T., 2018. Tree-, stand-and site-specific controls on landscape-scale patterns of transpiration. Hydrol. Earth Syst. Sci. 22 (1), 13–30.
He, Y., Qiu, Z., Liu, R., Tang, M., Wu, P., 2023. Impact of mulching on soil moisture and sap flow characteristics of jujube trees. Agronomy 13, 2799. https://doi.org/10.3390/agronomy13112799.
Hentschel, R., Hommel, R., Poschenrieder, W., Grote, R., Holst, J., Biernath, C., Gessler, A., Priesack, E., 2015. Stomatal conductance and intrinsic water use efficiency in the drought year 2003: a case study of European beech. Trees 30, 153–174.
Hosaini, Y., Homaee, M., Karimian, N.A., Saadat, S., 2009. Modelling vegetative stage response of canola (*Brassica napus* L.) to combined salinity and boron stresses. Int. J. Plant Prod. 3, 91–104.
Ibraimo, N.A., 2018. Water use of deciduous and evergreen tree nut crops: a case study using pecans and macadamias. PhD Thesis, University of Pretoria, South Africa.
Irmak, S., Mutiibwa, D., Irmak, A., Arkebauer, T., Weiss, A., Martin, D., Eisenhauer, D., 2008. On the scaling up leaf stomatal resistance to canopy resistance using photosynthetic photon flux density. Agric. For. Meteorol. 148, 1034–1044. https://doi.org/10.1016/j.agrformet.2008.02.001.
Ismanov, M., Henry, C., Espinoza, L., Francis, P., 2022. Modelling of soybean plant sap flow. Agric. Sci. 13, 658–673. https://doi.org/10.4236/as.2022.135043.
Korakaki, E., Fotelli, M.N., 2021. Sap flow in Aleppo pine in Greece in relation to sapwood radial gradient, temporal and climatic variability. Forests 12, 2.
Kumar, R., Hosseinzadehtaher, M., Hein, N., Shadmand, M., Jagadish, S.V.K., Ghanbarian, B., 2022. Challenges and advances in measuring sap flow in agriculture and agroforestry: a review with focus on nuclear magnetic resonance. Front. Plant Sci. 13, 1036078. https://doi.org/10.3389/fpls.2022.1036078.
Kumar, M., Joseph, G., Bhutia, Y., Krishnaswamy, J., 2023. Contrasting sap flow characteristics between pioneer and late-successional tree species in secondary tropical montane forests of Eastern Himalaya, India. J. Exp. Bot. 74 (17), 5273–5293. https://doi.org/10.1093/jxb/erad207.
Kume, T., Tsuruta, K., Komatsu, H., Shinohara, Y., Katayama, A., Ide, J.I., Otsuki, K., 2016. Differences in sap flux-based stand transpiration between upper and lower slope positions in a *Japanese cypress* plantation watershed. Ecohydrol 9, 1105–1116.
Leuning, R., 1995. A critical appraisal of a combined stomatal-photosynthesis model for $C_3$ plants. Plant Cell Environ. 18, 339–355.
Li, Y.H., Chen, Q., K.N., Wang, Z.X., 2022. The accuracy improvement of sap flow prediction in *Picea crassifolia* Kom. based on the back-propagation neural network model. Hydrol. Proc. https://doi.org/10.1002/hyp.14490.
Li, X., Zhai, J., Sun, M., Liu, K., Zhao, Y., Cao, Y., Wang, Y., 2024. Characteristics of changes in sap flow-based transpiration of poplars, locust trees, and willows and their response to environmental impact factors. Forests 15, 90. https://doi.org/10.3390/f15010090.
Mabhaudhi, T., Modi, A.T., Beletse, Y.G., 2014. Agricultural and forest meteorology parameterization and evaluation of the FAO-AquaCrop model for a South African taro (*Colocasia esculenta* L. Schott) landrace. Agric. For. Meteor. 192–93, 132–139. https://doi.org/10.1016/j.agrformet.2014.03.013.
Mashamaite, C.V., Pieterse, P.J., Mothapo, P.N., Phiri, E.E., 2021. *Moringa oleifera* in South Africa: a review on its production, growing conditions and consumption as a food source. S. Afr. J. Sci. 117 (3/4), 1–7.
McAusland, L., Acevedo-Siaca, L.G., R., Pinto, R.S., Pinto, F., Molero, G., Garatuza-Payan, J., Reynolds, M.P., Murchie, E.H., Yepez, E.A., 2023. Night-time warming in the field reduces nocturnal stomatal conductance and grain yield but does not alter daytime physiological responses. New Phytol. 239, 1622–1636. https://doi.org/10.1111/nph.19075.
McNider, R.T., Handyside, C., Doty, K., Ellenburg, W.L., Cruise, J.F., Christy, J.R., Moss, D., Sharda, V., Hoogenboom, G., Caldwell, P., 2015. An integrated crop and hydrologic modeling system to estimate hydrologic impacts of crop irrigation demands. Environ. Model. Softw. 72, 341–355.
Mokgehle, S., Araya, N., Mofokeng, M., Makgato, M., Amoo, S., Maboka, K., du Plooy, C., Araya, H., 2022. Regrowth response and nutritional composition of *Moringa oleifera* to cutting back in three agro-ecological zones in South Africa. Horticulturae 8, 963. https://doi.org/10.3390/horticulturae8100963.
Moriasi, D.N., Arnold, J.G., van Liew, M.W., Bingner, R.L., Harmel, R.D., Veith, T.L., 2007. Model evaluation guidelines for systematic quantification of accuracy in watershed simulations. Trans. ASABE 50 (3), 885–900.
Nash, J.E., Sutcliffe, J.V., 1970. River flow forecasting through conceptual models part I: a discussion of principles. J. Hydrol. 10, 282–290.
Noun, G., Lo Cascio, M., Spano, D., Marras, S., Sirca, C., 2022. Plant-based methodologies and approaches for estimating plant water status of Mediterranean tree species: a semi-systematic review. Agronomy 12, 2127. https://doi.org/10.3390/agronomy12092127.
Orgaz, F., Villalobos, F.J., Testi, L., Fereres, E., 2007. A model of daily mean canopy conductance for calculating transpiration of olive canopies. Funct. Plant Biol. 34, 178–188.
Ozcelik, M.S., Tomaskova, I., Surovy, P., Modlinger, R., 2022. Effect of forest edge cutting on transpiration rate in *Picea abies* (L.) H. Karst. Forests 13, 1238.
Poyatos, R., Granda, V., Molowny-Horas, R., Mencuccini, M., Steppe, K., Martinez-Vilalta, J., 2016. SAPFLUXNET: towards a global database of sap flow measurements. Tree Physiol. 36, 1449–1455. https://doi.org/10.1093/treephys/tpw110.
Pradiko, I., Rahutomo, S., Farrasati, R., Ginting, E.N., Hidayat, F., Syarovy, M., 2022. Transpiration of oil palm (*Elaeis guineensis* Jacq.) based on sap flow measurement: the relation to soil and climate variables. J. Oil Palm. Res. 35 (1), 168–184. https://doi.org/10.21894/jopr.2022.0035.
Rissanen, K., Lapa, G., Houle, D., Kneeshaw, D., Paquette, A., 2024. Large variation in the radial patterns of sap flow among urban trees. Agric. For. Meteor. 345, 109848. https://doi.org/10.1016/j.agrformet.2023.109848.
Roddy, A.B., Dawson, T.E., 2013. Novel patterns of hysteresis in the response of leaf level sap flow to vapour pressure deficit. Acta Hortic. 991, 261–267.
Safargalieva, A., Kochetkova, I., Makeeva, E., Shorgin, S., 2021. 2021 CEUR workshop proceedings (CEUR-WS.org). Workshop on Information Technology and Scientific Computing in the Framework of the 11th Int. Conf. Information and Telecommunication Technologies and Mathematical Modeling of High-Tech Systems (ITTMM-2021) (Moscow, Russian, 19–23 April).
Sakuratani, T., 1981. A heat balance method for measuring water flux in the stem of intact plants. J. Agric. Meteor. 37, 9–17.
dos Santos, C.S., Montenegro, A.A.D.A., dos Santos, M.A.L., Pedrosa, E.M.R., 2017. Evapotranspiration and crop coefficients of *Moringa oleifera* under semi-arid conditions in Pernambuco. R. Bras. Eng. Agric. Ambient. 21 (12), 840–845. https://doi.org/10.1590/1807-1929/agriambi.v21n12p840-845.
Schoppach, R., Chun, K.P., He, Q., Fabiani, G., Klaus, J., 2021. Species-specific control of DBH and landscape characteristics on tree-to-tree variability of sap velocity. Agric. For. Meteorol. 307, 108533.
Shackel, K.A., Johnson, R.S., Medawar, C.K., Phene, C.J., 1992. Substantial errors in estimates of sap flow using the heat balance technique on woody stems under field conditions. J. Am. Soc. Hortic. Sci. 117, 351–356.
Singh, V.K., Dwivedi, B.S., Shukla, A.K., Chauhan, Y.S., Yadav, R.L., 2005. Diversification of rice with pigeon pea in a rice-wheat cropping system on a Typic Ustochrept: effect on soil fertility, yield and nutrient use efficiency. Field Crops Res 92 (1), 85–105.
Suarez, J.C., Casanoves, F., Bieng, M.A.N., Melgarejo, L.M., di Rienzo, J.A., Armas, C., 2021. Prediction model for sap flow in cacao trees under different radiation intensities in the western Colombian Amazon. Sci. Rep. 11, 10512. https://doi.org/10.1038/s41598-021-89876-z.
Sun, X., Li, J., Cameron, D., Moore, G., 2021. On the use of sap flow measurements to assess the water requirements of three Australian native tree species. Agronomy 12, 52. https://doi.org/10.3390/agronomy12010052.
Vahrmeijer, J.T., Taylor, N.J., 2018. Quantifying citrus water use and water stress at orchard level. Measurement and modelling of seasonal citrus water use for different growth stages and canopy sizes. WRC Report No TT 772/2/18, Water Research Commission and Department of Agriculture Forestry and Fisheries, Pretoria, South Africa, Volume 2.
van Rooyen, N., Theron, G.K., Grobbelaar, N., 1986. The vegetation of the Roodeplaat Dam Nature Reserve. III. Phenological observations. S. Afr. J. Bot. 52, 153–158.
Villalobos, F.J., Testi, L., Orgaz, F., Garcia-Tejera, O., Lopez-Bernal, A., Gonzalez-Dugo, M.V., Ballester-Lurbe, C., Castel, J.R., Alarcon-Cabanero, J.J., Nicolas-Nicolas, E., et al., 2013. Modelling canopy conductance and transpiration of fruit trees in Mediterranean areas: a simplified approach. Agric. For. Meteorol. 171–172, 93–103.
Wan, Y., Peng, L., Anwaier, A., Shi, H., Li, D., Ma, Y., Shi, Q., 2024. Effects of meteorological factors and groundwater depths on sap flow density of *Populus euphratica* in a desert oasis, Taklamakan Desert, China. Front. Plant Sci. 15, 1330426. https://doi.org/10.3389/fpls.2024.1330426.
Wang, D., Gao, G.Y., An, J.X., Shao, Y.M., Lu, Y.H., Fu, B.J., 2022. Comparisons of three scaling up methods to estimate stand transpiration of a xerophytic shrub (*Salix psammophila*) in northern China. J. Hydrol. 608, 127593. https://doi.org/10.1016/j.jhydrol.2022.127593.
Wang, Y., Wei, X., del Campo, A.D., Winkler, R., Wu, J., Li, Q., Liu, W., 2019. Juvenile thinning can effectively mitigate the effects of drought on tree growth and water consumption in a young *Pinus contorta* stand in the interior of British Columbia, Canada. For. Ecol. Manag. 454, 117667.
Wei, X.G., Li, B., Guo, C.J., Wang, Y.K., He, J.Q., Liu, S.Y., et al., 2017. Identification of sap flow driving factors of jujube plantation in semi-arid areas in Northwest China. Int. J. Agric. Biol. Eng. 10 (2), 172–183.
West, R.R., Lada, R.R., MacDonald, M.T., 2023. Nutrition and related factors affecting maple tree health and sap yield. Am. J. Plant Sci. 14, 125–149.
Wheeler, W.D., Black, B., Bugbee, B., 2023. Assessing water stress in a high-density apple orchard using trunk circumference variation, sap flow index and stem water potential. Front. Plant Sci. 14, 1214429. https://doi.org/10.3389/fpls.2023.1214429.
Willmott, C.J., Matsuura, K., 2005. Advantages of the mean absolute error (MAE) over the root mean square error (RMSE) in assessing average model performance. Clim. Res. 30, 79–82.
Wu, S., Gu, X., Zheng, Y., Chen, L., 2023. Nocturnal sap flow as compensation for water deficits: an implicit water-saving strategy used by mangroves in stressful environments. Front. Plant Sci. 14, 1118970. https://doi.org/10.3389/fpls.2023.1118970.
Yang, L., Liu, H., Tang, X., Li, L., 2022. Tomato evapotranspiration, crop coefficient and irrigation water use efficiency in the winter period in a sunken Chinese solar greenhouse. Water 14, 2410. https://doi.org/10.3390/w14152410.
Zabihi, K., Singh, V.V., Trubin, A., Skova, I.T., Zenec, M.B., Surovy, P., Jakus, R., 2023. Sap flow as a function of variables within nested scales: ordinary least squares vs. spatial regression models. Environ. Res. Ecol. 2, 025002. https://doi.org/10.1088/2752-664X/acd6ff.

Zeng, X.M., Xu, X.L., Zhong, F.X., Xu, T.Y., Luo, W., Yi, R.Z., Li, X.Z., 2022. Use of gravimetric measurements to calibrate thermal dissipation probes with stem segments. Hydrol. Proc. 36, e14478. https://doi.org/10.1002/hyp.14478.
Zhang, J.G., He, Q.Y., Shi, W.Y., Otsuki, K., Yamanaka, N., Du, S., 2015. Radial variations in xylem sap flow and their effect on whole-tree water use estimates. Hydrol. Process. 29, 4993–5002.
Zhao, C.Y., Si, J.H., Feng, Q., Yu, T.F., Li, P.D., 2017. Comparative study of daytime and nighttime sap flow of *Populus euphratica*. Plant Growth Regul. 82, 353–362.
Zhou, H., Zhao, W., Zheng, X., Li, S., 2015. Root distribution of *Nitraria sibirica* with seasonally varying water sources in a desert habitat. J. Plant Res. 128, 613–622.